Progress in Lanthanides as Luminescent Probes

JEFF G. REIFENBERGER, PINGHAU GE, PAUL R. SELVIN

Physics Dept. and Biophysics Group, Univ. of Illinois, Urbana IL 61801

Contact info:
Loomis Laboratory of Physics, University of Illinois, 1110 W. Green St., Urbana, IL 61801,
(tel.) 217-244-3371; (fax) 217-244-7187
selvin@uiuc.edu

Key words: Fluorescence Resonance Energy Transfer, Lanthanide, Luminescence,

Published in:

Reviews in Fluorescence 2005, Vol. 2

Edited by Chris D. Geddes, Joseph R. Lakowicz

Springer

Abstract:

Using luminescent lanthanides, instead of conventional fluorophores, as donor molecules in resonance energy transfer measurements offers many technical advantages and opens up a wide-range of new applications. Advantages include farther measurable distances (~100 Å) with greater accuracy, and insensitivity to incomplete labeling. We have also generated new luminescent lanthanide compounds with various advantages over more conventional probes. Applications highlighted include the study of ion channels in living cells and measuring *in vitro* conformation changes within smooth muscle myosin.

Introduction to Lanthanide probes:

Luminescent lanthanide chelate complexes have unusual spectral characteristics when compared to typical organic fluorophores. These include millisecond lifetimes, sharply spiked emission spectra, high quantum yield, unpolarized emission, and a broad range of emission energies extending from the blue to the red part of the spectrum. Lanthanides are therefore an alternative to organic fluorophores particularly where there are problems of background autofluorescence [1, 2] and as donors in fluorescence (luminescence) resonance energy transfer to measure nanometer conformational changes and binding events within proteins [3-5].

First we briefly discuss the luminescent and photophysical characteristics of lanthanides as well as new lanthanide compounds that are more soluble in water, followed by a brief review of FRET theory and measurement, highlighting those areas where lanthanides differ from conventional probes. We then show a number of applications where LRET has enabled new types of systems to be studied: ion channels in living cells and the molecular motor myosin in vitro.

Structural and Photophysical Characteristics of Lanthanide Probes:

Figure 1a shows a typical polyaminocarboxylate chelate, DTPA-cs124, in which a Tb^{3+} atom is bound. It contains an organic chromophore (carbostyril 124), which serves as an antenna or sensitizer, absorbing the excitation light and transferring the energy to the lanthanide ion. An antenna is necessary because of the extremely weak absorbance of the lanthanide (1 $M^{-1}cm^{-1}$, or 10^4-10^5 times smaller than conventional organic fluorophores). The complexes also contain a chelate (DTPA) which serves several purposes, including binding the lanthanide tightly, shielding the lanthanide ion from the quenching effects of water, and acting as a scaffold for attachment of the antenna and a reactive group (either amine or thiol), the latter for coupling the chelate complex to biomolecules. Once bound to a biomolecule, the probe can be used in resonance energy transfer application (if an acceptor dye is chosen to be around) [3, 5-17].

In general, there are two types of lanthanide complexes. In the first type of complex, the chelate backbone serves as both the coordination site for the lanthanide ion and the sensitizer, to absorb photons and transfer energy to the bound lanthanide. Chelates used in this type of complex include β-diketone, pyridine derivatives, cryptands, terphenyl-based compounds (see figure 1b for an example) [18, 19]. In the second type of lanthanide complexes, which will be the focus of this chapter, the complexes have relatively distinct components such that the chelate, antenna, and reactive group are separate components. An example of this second type of

structure was shown figure 1a. This second approach has the advantage of allowing for the optimization of both the structure of the coordination site and the sensitizer separately.

Fig. 2a shows the emission spectra and Fig. 2b shows the excited state lifetime characteristics of the DTPA-cs124 bound to either terbium or europium. These two are, by far, the most useful lanthanides. Dy and Sm are the only other two lanthanides that emit in the visible, but with much weaker intensity [20]. Excitation of the antenna is in the ultraviolet, typically utilizing a pulsed nitrogen laser (337 nm), although flash lamps can also be used. Emission is in the green for Tb^{3+} and in the red for Eu^{3+}. This large Stokes shift enables easy discrimination against excitation light. As seen in figure 2a and 2b, Eu^{3+} and Tb^{3+} emission are sharply spiked in wavelength, with long (millisecond) excited state lifetimes. These attributes are important for resonance energy transfer applications (see below). The sharply-spiked spectra occur because emission is atomic-like and the chelate shields the atom from broadening effects of the solvent.

The sharply-spiked spectra occur because emission arises from high-spin—high-spin transition within the lanthanide atom. Tb^{3+} emission occurs between a $^5D_4$ excited state to a ground state of ^7F_J (J = 0 - 6) while Eu^{3+} emission is from a $^5D_0$ excited state to a ^7F_J (J = 0 - 6) ground state [21]. The long lifetimes for both lanthanides occur because the ground state and excited state involve electrons in the 4f shell and hence the transitions are formally parity forbidden [21]. Nevertheless, a small admixture of 5d electrons makes the transitions possible. Despite the unusual nature of the atomic states, emission within the lanthanides primarily arises from electric dipole transitions with the exception being the $^5D_0$ to $^7F_1$ transition in Eu^{3+}, which arises from a magnetic dipole [21-23]. This is important because electric dipole transitions are the same mechanism used by organic fluorophores. Hence the electric field produced by a lanthanide donor (regardless of whether it is from an electric or magnetic dipole) and by an organic donor have the same distance dependence, i.e. they both decrease as $1/R^3$ for distances << wavelength of light. Ultimately, this leads to the same distance dependence, R^{-6}, for resonance energy transfer measurements using either lanthanides or organic donors.

Another unique spectral feature of lanthanides when they are bound to a chelate-antenna complex is that the emitted light is unpolarized [23]. This is important when lanthanide complexes are used in energy transfer as donors. Energy transfer not only has a R^{-6} distance dependence between the donor and the acceptor, but there is also an orientational dependence as well. For example if the donor and acceptor are rigid and perpendicular to each other, then there will be no energy transfer from the donor to the acceptor no matter how close the two dyes may be to each other. Until recently, it had always been assumed that the emission of the Tb^{3+} and Eu^{3+} within the chelate-antenna would be mostly unpolarized due to the nature of the initial and final quantum states of the lanthanides. Reifenberger et al. froze lanthanide-chelate-antenna complex in a glycerol-water mixture and were able to measure the anisotropy of their emission (an anisotropy near zero corresponds to unpolarized emission). They found that the anisotropy of Eu-DTPA-cs124 was very small and actually zero in some of the transitions. Tb-DTPA-cs124's emission was also unpolarized. Figure 3 and figure 4 shows the anisotropy of Eu^{3+} and Tb^{3+} when bound to DTPA-cs124. (The anisotropy was essentially the same for both Eu^{3+} and Tb^{3+} bound to another chelate-antenna complex, TTHA-cs124 [23].

The emission quantum yield for Terbium or Europium in the chelates is also quite high [24]. This is important because the efficiency of energy transfer is proportional to the donor quantum yield (Equations 3 and 5 below). By lanthanide quantum yield, Q_{Ln}, here we mean the

probability that the lanthanide will emit a photon given that the *lanthanide* is excited. This definition is very similar to that used with conventional fluorophores although there is a subtlety. Lanthanide excitation is a two step process: the antenna absorbs a photon, and then passes this energy onto the lanthanide with some finite probability ($\equiv Q_{transfer} \leq 1$) (Fig. 3). The lanthanide then emits with some probability – i.e. the quantum yield mentioned above, Q_{Ln}. The overall probability that the lanthanide will emit a photon (Q_{total}), given that an excitation photon was *absorbed* by the complex (antenna), is:

$$Q_{total} = Q_{Ln} \times Q_{transfer} \quad (1)$$

Figure 5 is a diagram of the process described in equation 1. For organic fluorophores $Q_{transfer} \equiv 1$ and hence $Q_{total} = Q_{Ln}$. For Tb^{3+} and Eu^{3+} in polyaminocarboxylate chelates such as in Fig 1a, $Q_{transfer} = 0.4 - 0.75$ and $Q_{total} = 0.1\text{-}0.4$ [24]. In any case, the efficiency of energy transfer (related to R_o, the distance at which half the donor's energy is transferred to the acceptor, see Equation 5) is proportional to Q_{Ln}, and Q_{total} is only relevant in that it affects the total brightness of the sample.

In order for the lanthanides to be useful in bioassays, the chelates must have a reactive group for attachment to biomolecules. Fortunately, the standard reactive groups can be coupled to the chelates: amine reactive groups such as isothiocyanates [25] and thiol-reactive groups such as maleimides, bromoacetamides, pyridyl dithio groups [26] have been made for the polyaminocarboxylate chelates. The reactive groups, can, however, lead to more complicated photophysics in that they can interact with the antenna molecules or adopt multiple conformations, leading to multi-exponential lanthanide decays, particularly with terbium [26].

Several amine-reactive or thiol-reactive lanthanide chelates have been synthesized (figure 6 and figure 7) in our lab. Due to the fact that DTPA dianhydride is commercially available and not expensive, DTPA dianhydride is widely used as the backbone of the structure in which both an antenna molecule and reactive group are attached. Antenna molecules containing a free amino group are reacted with one of the two dianhydride bonds to attach the antenna molecule to the backbone. The remaining anhydride group is either converted into an amine-reactive or a thiol-reactive functional group via either an alkyl diamine or a hydrazine linker.

We have synthesized two different amine reactive complexes in our lab. The first, **AR1** shown in figure 6a, is an in situ formed intermediate formed during synthesis and cannot be separated [25]. The second, **AR2** shown in figure 6b can rapidly react with a free amine group at pH ~9. Figure 7 shows the main thiol-reactive forms of chelate-antenna complexes, which include maleimide (**TR1, TR2**), pyridyldithiol (**TR3**), MTS (methanethiosulfonate, **TR4, TR5**), and haloacetyl amide (**TR6, TR7, TR8**). The maleimide form has the advantage of a quick, efficient, and irreversible reaction with thiols. **TR1** has been used as a donor in LRET experiments in the studies of muscle proteins and ion channels [15, 17, 27]. MTS is a labeling reagent frequently used in ion channel studies [28]. While having two lifetime components, the Tb^{3+} and Eu^{3+} complexes of purified MTS chelate **TR5**, have shown a predominant long lifetime component with an amplitude greater than 90%. The long lifetime component remains even after labeling to proteins and ion channels [29] . Two different haloacetyl amide chelates have been synthesized in our lab as well, bromoacetamide and iodoacetamide. The bromoacetamide chelate, **TR6**, has exhibited single exponential decay in its emission measurement with a lifetime

of 1.51 ms. Upon reaction with a reduced form of glutathione, the adduct still exhibits a single exponential decay in its lifetime [30]. However, the disadvantage of this form of the chelate is that it is not very reactive towards thiols and requires relatively high pH, which can also denature the proteins that are being labeled [31]. The iodoacetamide chelates, **TR7** and **TR8**, have increased reactivity and labeling can occur at a neutral pH. However their adducts to biomolecules often show bi- or tri- exponential decay [29].

Modified chelates and antennas and their effect on Lanthanide luminescence:

Chelates

The most commonly used chelate is DTPA (diethylenetriaminepentaacetic acid) attached to an antenna molecule, cs124. Other polyaminocarboxylates have also been used (see figure 8) to attach to cs124 [32]. These chelates have shown sensitization to both terbium and europium except TETA-cs124 (Table 1). Tb^{3+} and Eu^{3+} can normally take 9 coordination atoms in their inner sphere [21]. DTPA-cs124 and DOTA-cs124 are 8-dentate chelates and therefore their lanthanide complexes have ~1 coordinated water molecule to the ions. Because of the solvent quenching effect of water, their lanthanide complexes, particularly for Eu^{3+}, have shortened lifetimes compared to the theoretical maximums. In contrast, TTHA-cs124 is a 10-dentate chelate, which can provide better protection to lanthanide ions from solvent attack. As the result, the lanthanide complexes of TTHA-cs124 have significantly longer lifetimes compared to that of DTPA-cs124 and DOTA-cs124 with calculated number of water bound in the inner sphere at ~0.2.

Antenna

Substituted cs124 derivatives have been used as antenna molecules to lanthanide ions (Fig. 9) [30, 33]. Among these cs124 derivatives, compounds **d1-d5** introduced an additional hydrophilic group on the aromatic ring structure, making them more soluble in aqueous media, especially for **d4**. The light absorption and energy transfer to the lanthanide of an antenna molecule is a complex process and the mechanism has not been fully characterized [34-37]. It is therefore difficult to predict how the antenna's structure will affect the photophysics of the corresponding lanthanide-chelate complex.

Table 2 lists the lifetimes and relative intensity of the Tb^{3+} and Eu^{3+} complexes of chelates made from various cs124 derivatives. Generally, the Tb^{3+} and Eu^{3+} complexes of these chelates have comparable emission brightness to the benchmark chelate, DTPA-cs124. By introducing hydrophilic groups to the sensitizers, the chelates derived from **d1**, **d4**, **d3**, **d5**, **d2** possess increased solubility in water, especially in the case of **d4**. Although they show comparable emission brightness to the reference complex, DTPA-cs124, they often have shorter lifetimes. Contrary to this trend, Tb^{3+}-DTPA-**d4** shows slightly longer lifetime, and its brightness is about 62% that of Tb^{3+}-DTPA-cs124. Clearly, the introduction of 6-SO_3H on cs124 has no dramatic effect on the emission properties of its lanthanide complex.

In some cases the cs124 derivatives are only luminescent with Eu^{3+}. Both the DTPA and TTHA chelates of **d8** do not cause Tb^{3+} to luminesce [33]. However, their Eu^{3+} complexes exhibit 3 and 1.17 times luminescent intensity than the corresponding DTPA-cs124 complexes.

It is also observed that with a substitute on the 3-postion of cs124 ring, its lanthanide chelate tends to be silent to Tb^{3+} and active to Eu^{3+}[33].

The Tb^{3+} complexes with the chelates of 6- or 8-CH_3 cs124 derivatives, especially the 8-CH_3 derivative, have longer lifetimes than DTPA-cs124 (1.74 ms vs. 1.53 ms). This suggests that higher lanthanide quantum yield was achieved in these complexes. Increased lanthanide quantum yield could result from either a decrease in solvent quenching or a decrease in energy back transfer to the antenna. The number of solvent molecules coordinated to the lanthanide ion in Tb^{3+}-DTPA-**d4** was measured using the method of Horrocks and Sudnick [38] in both H_2O and D_2O. The calculated number of water for both the chelate and the reference complex, Tb^{3+}-DTPA-cs124 is all 1.1, indicating that there is no difference in solvent quenching. Clearly, the higher quantum yield is achieved from a decrease of energy back-transfer from the excited Tb^{3+} to **d4**. In contrast, no energy back-transfer was observed for unsubstituted cs124 chelates [32].

Lanthanide-based Resonance Energy Transfer:

Theory of LRET

Lanthanides were first used in resonance energy transfer experiments by Horrocks and co-workers in the 1970s [39, 40]. A lanthanide was bound to a calcium-binding protein and used as a donor to transfer energy to a freely diffusing or specifically bound metal (e.g. Co). The lanthanide was excited either directly, using a powerful laser, or through a tryptophan near the lanthanide that acted as an antenna molecule. Because of the weak absorption of the metal acceptor, the donor-acceptor dipole coupling and hence measurable distances, were small (a few Angstroms). However, the work first demonstrated the idea of using lanthanides for resonance energy transfer and was useful for measuring small distances (~10 Å). Meares and co-workers in the early 1980s then used lanthanides bound to artificial chelates as donors to transfer energy to organic acceptors, in which either the donor or acceptor was free to diffuse [3]. The use of organic acceptors, which have strong absorbance where the donor emits, dramatically increased the measurable distance range (discussed further below). The primary goal in these experiments was to measure how close two probes could approach each other as one or both diffused.

LRET (luminescence, or lanthanide-based resonance energy transfer), as used in my laboratory and elsewhere, relies on the same fundamental mechanism as FRET, but instead of using two organic-based probes, uses a lanthanide donor and an organic acceptor [41], both specifically bound to a biomolecule. Both LRET and FRET utilize visible light (roughly 500 nm wavelength), yet achieve sub-nanometer resolution. In both techniques, a luminescent (fluorescent) probe, called the donor, transfers energy via a dipole-dipole interaction to a second structurally-different probe, called the acceptor [42-45]. At distances less than the wavelength of light, λ, the electric field predominantly drops off as R^{-3}. (For $R >> \lambda$, the electric field is proportional to R^{-1}). An acceptor, if nearby and containing energy levels corresponding to the frequencies of the oscillating electric field, can interact with this field, absorb the energy, and become excited. The probability of the acceptor being excited depends on the square of the electric field strength and hence decays as R^{-6} for $R << \lambda$, the relevant distance scale in FRET/LRET ($\lambda \approx 500$ nm). Energy transfer also depends on how well the acceptor energy levels match the frequencies of the donor (the so-called spectral overlap term – Equation 6, below). Finally, energy transfer may also depend on the orientation of the donor and acceptor (the κ^2

term – Equations 5 and 7) because the electric field of the donor may be polarized and anisotropic. FRET and LRET can measure distances between the probes over a range of 20-100 Å. This high spatial resolution is possible, even with optical photons, because the amount (or more precisely, the efficiency) of energy transfer (*E*) is a strong function of distance between the donor and acceptor fluorophores.

The efficiency of energy transfer, *E*, is defined as the probability that an excited donor will return to the ground state by giving its energy to an acceptor. This can be written as:

$$E = \frac{k_{et}}{k_{et} + k_{nd}} = \frac{1}{1 + k_{nd}/k_{et}} = \frac{1}{1 + 1/k_{et}\tau_D} \tag{2}$$

where k_{et} is the rate of energy transfer and is distant-dependent, and k_{nd} is the rate of all other donor decay processes, such as radiative and non-radiative rates of donor decay. These latter processes clearly do not depend on the donor-acceptor distances. The donor lifetime in absence of acceptor is τ_D. Note that *E* depends on the ratio k_{et} to the other processes, but does not depend on the absolute donor lifetime. In FRET, donor rates (or lifetimes) and energy transfer rates are in the nanosecond range whereas in LRET they are in the millisecond range. As a side point, if the distance between the probes changes slowly on the FRET time-scale, but quickly on the LRET timescale, the two techniques can give dramatically different energy transfer efficiencies. Indeed, one signature of such dynamics is if LRET gives a much higher *E* than FRET [46].

Because the rate of energy transfer depends on R^{-6} distance between donor and acceptor, Equation 2 can be rewritten as:

$$E = \frac{1}{1 + \left(\frac{R}{R_o}\right)^6} \tag{3}$$

where R_o is the distance at which half of the energy is transferred and is generally 20-60 Å and typically 40-70 Å for LRET. The steep distance dependence, R^{-6}, arises because induced-dipole induced-dipole interactions depend on R^{-6}. (In quantum mechanical terms we talk instead of transition dipole moments, which also leads an R^{-6} dependence.) By knowing or calculating R_o, and measuring *E*, the distance between the probes can be found by the rearranging the terms in equation 3.

$$R = Ro\left(\frac{1}{E} - 1\right)^{1/6} \tag{4}$$

An important limitation of equation 4 is that R_o is often not known precisely, which limits the ability of FRET to measure absolute distances. R_o is typically calculated based on the spectral

properties of the donor and acceptor, but also depends on the orientation of the donor and acceptor, which is often not precisely known. (For details, see [41, 47]). Consequently, if R_o can be determined or calculated and *E* measured spectroscopically, then FRET/LRET can be used as a spectroscopic ruler to determine distances [48].

R_o is usually calculated from the spectral properties of donor and acceptor [49]:

$$Ro = 0.21\left(Jq_D n^{-4}\kappa^2\right)^{1/6} \quad \text{(in Angstroms)} \tag{5}$$

$$J = \int \varepsilon_A(\lambda) f_D(\lambda)\lambda^4 d\lambda \Big/ \int f_D(\lambda) d\lambda \quad \text{in } \underline{\text{M}}^{-1}\text{cm}^{-1}\text{nm}^4 \tag{6}$$

where *J* is the normalized spectral overlap of the donor emission (f_D) and acceptor absorption (ε_A in units of $\underline{\text{M}}^{-1}\text{cm}^{-1}$ where $\underline{\text{M}}$ is units of Moles/liter), q_D is the quantum efficiency (or quantum yield) for donor emission in the absence of acceptor (q_D = number of photons emitted divided by number of photons absorbed), n is the index of refraction (1.33 for water; 1.29 for many organic molecules) and κ^2 is a geometric factor related to the relative orientation of the transition dipoles of the donor and acceptor and their relative orientation in space. Note that for LRET, q_D in Equation 5 is Q_{Ln}, and not $Q_{overall}$ (Equation 1). This is because Q_{Ln} determined the strength of the donor's electric field, not $Q_{overall}$.

The orientation term, κ^2, in R_o, is often a source of uncertainty in FRET measurements. It is defined as

$$\kappa^2 = \left(\cos\theta_{DA} - 3\cos\theta_D \cos\theta_A\right)^2 \tag{7}$$

where θ_{DA} is the angle between the donor and acceptor transition dipole moments, θ_D (θ_A) is the angle between the donor (acceptor) transition dipole moment and the R vector joining the two dyes. By measuring the polarization of donor and acceptor emission, constraints on these angles can often be imposed, reducing --though usually not completely eliminating-- the uncertainty in κ^2. κ^2 ranges from 0 if all angles are 90 degrees, to 4 if all angles are zero degrees, and equals 2/3 if the donor and acceptor rapidly and completely rotate during the donor excited state lifetime [47]. If the donor emission is unpolarized as is the case for terbium, and mostly true for europium [23], and the acceptor is completely rigid and either parallel (κ^2 = 2/3) or perpendicular (κ^2 = 1/3) to the radius vector, then $1/3 < \kappa^2 < 2/3$. This limits the worst case error in R_o to –11% +12% if one simply assumes κ^2 = 2/3. Furthermore since the lanthanides have millisecond lifetimes, the acceptor will very likely rotate during this time, making κ^2 very close to 2/3. Hence, the error in distances measured via LRET due to the orientation factor is essentially negligible. This in turn makes the distance determination via LRET generally more accurate than FRET since the orientation factor in FRET is often poorly known.

Finally, R_o is also proportional to J, the spectral overlap. The lanthanides have highly spiked emission spectra in regions where several excellent dyes absorb (Fig. 2a) – e.g. the Tb^{3+} 490 nm emission peak overlaps well with Fluorescein, Green Fluorescent Protein, and Alexa 488 absorption; the Tb^{3+} 546 nm peak overlaps with Cy3, Tetramethylrhodamine, Alexa 546, and R-Phycoerythrin absorption. The Eu^{3+} 617 nm emission peak overlaps with Cy5, Alexa 633, and Allophycocyanin absorption. Consequently, J for LRET can be unusually large. When combined with a high Q_{Ln}, the R_o in LRET can also be quite large (Table 3).

Measuring E

In Fig. 10, an energy transfer experiment between a terbium labeled DNA and rhodamine-labeled DNA complement is shown [50]. This example highlights various ways of measuring energy transfer. In FRET and LRET, there are several ways of measuring E: a reduction in donor intensity in the presence of acceptor (due to some of the donor's energy going to the acceptor instead of into donor emission); by a decrease in donor excited state lifetime (energy transfer to the acceptor is an additional relaxation pathway of the donor's excited state); or by an increase in acceptor fluorescence (the acceptor is receiving energy from the donor and converting this energy into acceptor fluorescence). In LRET, E can also be measured via the sensitized emission lifetime (see below). In FRET, but not LRET, E can also be measured by an increase in the photostability of the donor in the presence of the acceptor because energy transfer to the acceptor decreases the donor's excited-state lifetime and photobleaching is generally proportional to the amount of time the dye spends in its excited state. Finally FRET and potentially LRET can be measured by an increase in donor intensity following photodestruction of the acceptor [51].

The efficiency of energy transfer (E) is then:

$$E = 1 - \frac{I_{D_A}}{I_D} = 1 - \frac{\tau_{D_A}}{\tau_D} = 1 - \frac{\tau_{A_D}}{\tau_D} = 1 - \frac{\tau_D^{bl}}{\tau_{D_A}^{bl}} \tag{8}$$

where I_{D_A}, τ_{D_A}, $\tau_{D_A}^{bl}$ are the donor's intensity, excited state lifetime, and photobleaching time constant in the presence of acceptor, and I_D, τ_D, and τ_D^{bl} are the same parameters in the absence of acceptor. τ_{A_D} is the lifetime of the sensitized emission of acceptor and is discussed further below.

Although using absolute intensities I_{D_A} and I_D is conceptually easy, it involves matching concentrations of two different samples and hence is prone to titration errors. Lifetime measurements avoid this problem and also are able to resolve multiple species with different energy transfer efficiencies. Fig. 10c shows a single exponential donor-only lifetime, which is reduced upon hybridization with a DNA strand containing an acceptor. Starting with a single-exponential donor-only lifetime is not essential but significantly simplifies the analysis of complex donor-acceptor mixtures. Titrating in with sub-stoichiometric amounts of acceptor strand leads to two populations and hence a bi-exponential donor decay: a donor-only

unhybridized strand (τ_D = 2.1 msec) and donor-acceptor double-stranded DNA (τ_{D_A} = 330 μsec). The amount of energy in the donor-acceptor pair can be calculated in equation 8 using the 330 μsec lifetime and the donor-only lifetime of a terbium-DNA hybridized to an unlabeled complementary DNA, which is 2.8 msec (data not shown). The relative populations of the two species can be determined by their pre-exponential amplitudes. Titrating in more acceptor strand increases the amplitude of the short time component but leaves its lifetime unchanged, as expected.

In LRET, E can also be measured by measuring the lifetime of the sensitized emission of acceptor – Fig 10c, curve D. The donor is excited by a pulse of light, the direct acceptor emission decays in nanoseconds, and any acceptor emission after this initial delay is therefore due only to energy transfer received by the acceptor from the long-lived donor. Its lifetime, τ_{A_D}, will follow the donor's lifetime, τ_{D_A}. Importantly, τ_{A_D} can be measured without contaminating background from either direct acceptor fluorescence (via temporal discrimination), or from donor emission (via spectral discrimination). The latter is possible because the donor is sharply spiked in emission spectra, including regions where the donor is dark, yet where the acceptor fluoresces. For example, Terbium is dark around 520 nm and 570 nm, where fluorescein and tetramethylrhodamine emit, respectively. Consequently, the temporal decay of the acceptor's sensitized emission can be measured with no background from either donor leakage or direct acceptor leakage. This sensitized emission lifetime is a very powerful advantage of LRET because it only arises from donor-acceptor pairs. In Fig. 10b, curve D, the sensitized emission lifetime is seen to closely match the short component of the donor lifetime yet does not have "contamination" from the donor-only DNA strands. The pre-exponential amplitudes of the sensitized emission decay correspond to the population of *excited* acceptors. Therefore in a multi-exponential decay, corresponding to a distribution of donor-acceptor pairs, the pre-exponential terms are the product of the individual energy transfer efficiencies and their populations [52]. This is in contrast to the donor decay in which the amplitudes are just proportional to populations.

Energy transfer also increases the acceptor's emitted intensity. In the donor-acceptor labeled sample, *E* can therefore be measured by comparing the residual donor fluorescence intensity, I_{D_A}, to the acceptors emission due to energy transfer I_{A_D}, and normalizing by their quantum yields (q_i's):

$$E = \frac{\dfrac{I_{A_D}}{q_A}}{\dfrac{I_{D_A}}{q_D} + \dfrac{I_{A_D}}{q_A}} \qquad (9)$$

The numerator is the number of acceptor excitations, and the denominator is the total number of excitations, i.e. the number of donor excitations that lead to donor emission (first term, denominator) and the number of acceptor excitations (second term, denominator). It is necessary to normalize the emission intensities by the quantum yields because *E* is measured in terms of

excitations, i.e. E is the fraction of the donor excitations that get converted into acceptor excitations.

Fig. 10c shows the *time-delayed* emission spectra of the donor and donor-acceptor complex (corresponding to curve C in Fig. 10b), which can be used to determine the two intensities in equation 9. The donor-acceptor sample is excited using a short excitation pulse and emission is detected after a few tens of microsecond delay. This procedure eliminates all prompt fluorescence of the acceptor. It also eliminates any contribution from acceptor-only species, if present, as well as any direct fluorescence from the antenna, both of which have nanosecond lifetime. The donor-acceptor spectra are then fit to the sum of a donor- and acceptor- spectra, with I_{D_A} being the area due to donor emission and I_{A_D} equal to the area under the acceptor emission. Note that the absolute concentrations of the donor-only species, the acceptor-only species, and the donor-acceptor species are irrelevant. In practice, the curve-fitting is done as follows: The donor-only spectra and donor-acceptor spectra are normalized at the 490 nm peak – or any point where there is no acceptor fluorescence. The donor-only curve is then subtracted from the donor-acceptor spectra and the difference is the sensitized emission curve, with area I_{A_D}. This should have the same shape as an acceptor-only emission spectra. I_{D_A} is simply the area under the donor-curve. Although we always take a donor-only spectrum as a control, we have found that the spectral shape of Tb-DTPA-cs124 does not change under any condition tested, and hence, a donor-only spectra taken once, is very likely to remain unchanged.

There are two additional points needed to properly use equation 9. First, the emission spectra must be corrected for wavelength sensitivity of the detector. This is done via conventional means using an emission source (standard lamp or a dye) whose emission spectra is known [43]. Second, the donor and acceptor quantum yields must be measured. Fortunately, we have recently determined the quantum yield of Tb^{3+} and Eu^{3+} in free polyaminocarboxylate chelates [24]. The quantum yield of lanthanide chelates bound to biomolecules can then simply be determined by comparing lifetimes to the free chelates. Acceptor quantum yields can be measured by conventional means: intensity or lifetime comparison to a standards such as Fluorescein (QY = 0.93 in 1 N NaOH [53]), Tetramethylrhodamine (QY = 0.58 in 10 mM Na-phosphate buffer, pH 7.46, 80 mM NaCl, room temperature [54]), or SulfoRhodamine 101 (QY = 1, lifetime = 4.36 nsec, in methanol [55]).

The importance of equation 9 is that it allows accurate measurement of relatively small amounts of energy transfer (distances > R_O). It is also interesting to note, though not widely appreciated, that by combining equations 4, 5, and 9, the calculated distance depends only on the acceptor quantum yield, and *not* on the donor quantum yield:

$$R = C\left(\frac{I_{D_A} q_A}{I_{A_D}}\right) \tag{10}$$

where C is simply all the constants in R_O except q_D. Finally, Equations 9 and 10 can also be used in conventional FRET, but here the direct excitation of acceptor must first be subtracted off [56].

Advantages of LRET

The primary drawbacks of FRET, i.e. using conventional dyes, are several-fold. a) FRET operates over a limited distance range, typically < 75 Å, because of the relatively small size of R_o and limited signal/background at larger distances (although see [57] and Alexa dyes from Molecular Probes Inc., www.probes.com). (b) *E* generally depends on the orientation of dyes, as well as their relative distance. (c) The finite size of the probes and uncertainty of dye position with respect to biomolecule attachment site, causes the measured dye-dye distances different than the protein-protein distances. (d) Incomplete labeling of biomolecules with dyes can make it difficult to extract distances.

While relying on the same fundamental dipole-dipole mechanism, LRET has many technical advantages over FRET. These include greater: distance accuracy and range; the ability to resolve multiple donor-acceptor distances; a greater ability to isolate signal from biomolecules labeled with both donor and acceptor, even in the presence of biomolecules labeled only with donor or only with acceptor; and less sensitivity of energy transfer to orientation of dyes. Like FRET, LRET shares the problem of sizable probes. (The chelate's atomic structure has also been determined [58], and it is roughly the same size as conventional fluorescence dyes). The linker in LRET is often somewhat shorter than for FRET probes [26].

The fundamental advantages of LRET arise because the donor emission is long-lived (Fig 2b; msec compared to nsec of acceptor or conventional dyes), sharply-spiked emission (Fig. 2a; peaks of a few nanometer width), has a high quantum yield, and is unpolarized.

1. *An order of magnitude greater accuracy in distance-determination can be achieved with LRET* because the energy transfer process is dominated by the distance between the donor and acceptor, and their relative orientations play only a minor role in determining energy transfer efficiency. A worst case scenario is 12% uncertainty in distance determination due to orientation effect. This advantage is because terbium, and usually europium emission is unpolarized [23]. This contrasts to FRET where the errors due to orientation effects can be unbounded. We have shown that angstrom changes due to protein conformational changes can readily be measured with LRET [15, 17].
2. *A 50-100-fold improvement in signal to background (S/B) can be achieved with LRET.* Specifically, energy transfer can be measured with essentially no contaminating background, a stark-contrast to many FRET dye pairs. By temporal and spectral discrimination, donor emission and acceptor emission – both intensity and lifetime — can be independently measured. This leads to dramatically improved signal to background compared to most FRET pairs. Specifically, in LRET the acceptor emission due *only* to energy transfer —the sensitized emission—can be measured with no background. Contaminating background in FRET when trying to measure energy transfer via an increase in acceptor fluorescence, arises from two sources: direct excitation of the acceptor by the excitation light (called direct acceptor fluorescence) and donor emission at wavelengths where one looks for acceptor emission. In LRET both sources are eliminated. For example, by choosing an acceptor such as fluorescein and looking around 520 nm, donor emission is dark (Fig. 2a). By using pulsed excitation and collecting light at 520 nm only after a few tens of microseconds, all the direct acceptor emission (which has nanosecond lifetime) has decayed away. Any acceptor photons emitted after a few microseconds following the excitation pulse, is therefore due only to

energy transfer. Small backgrounds mean small signals, corresponding to relatively large distances (10 nm), can be measured.

3. *Samples that contain donor-only or acceptor-only can be spectrally and temporally discriminated against.* Often when labeling proteins, particularly in living cells, one gets an unknown distribution of donor-donor, donor-acceptor, acceptor-acceptor mixture. In FRET this makes distance-determination difficult. In LRET, sensitized emission from acceptor arises only from donor-acceptor labeled complex (see preceding paragraph). Energy transfer of this donor-acceptor labeled complex can then be determined by comparing the lifetime of sensitized emission (τ_{A_D}), which decays with micro- to millisecond lifetime of donor that is transferring energy to the acceptor, with the donor-only lifetime. The ability to measure energy transfer even in complex labeling mixtures is essential for the LRET studies on ion channels presented below.

Instrumentation and Applications:

The instrumentation to perform LRET is relatively simple, although slightly more complex than conventional steady-state fluorimeters. The general requirements are a pulsed UV excitation source and time-resolved detection. The pulsed excitation source is usually a Nitrogen laser (337nm, 5 nsec pulse-width typical, 20-50 Hz repetition rate). For lifetime measurements, a photomultiplier tube with suitable color filters and counting electronics is used. For time-delayed spectra, a spectrometer, typically utilizing diffraction gratings, and either a time-gated photomultiplier tube or preferably a CCD, gated either electronically or with a mechanical chopper, is used. A schematic of the instrument built in our laboratory is shown in Figure 11 and details are given elsewhere [24, 59].

The technical advantages of LRET open up many applications. Here we highlight two representative examples that use LRET *in vivo* and *in vitro*.

Ion channels:

We have used LRET to measure conformational changes in the Shaker potassium ion channel, a voltage-gated channel involved in nerve impulses. In many ways this is an extremely demanding use of LRET. The measurement is on a living cell (Xenopus oocytes) and hence purification of completely labeled donor-acceptor species is not possible. A heterogeneous mixture of labeled proteins exists, all in the presence of non-specific labeling to other membrane components. Furthermore, two distances are expected to exist (see below) and the distance changes (as a function of voltage – see below) are quite small – a few angstroms. The technical advantages of LRET help overcome these difficulties.

The channel is a transmembrane protein, consisting of four identical subunits (Fig. 12a, b) with 4-fold symmetry. Each subunit contains six transmembrane spanning segments, S1-S6 (Fig. 12c). A pore, or channel, is formed at the intersection of the four subunits, which is opened or closed, i.e. "gated", depending on the voltage across the cell membrane. At the resting transmembrane potential of approximately –60 mV the pore is closed. Upon depolarization to approximately 0 mV, the protein undergoes a conformational change that ultimately leads to an opening of the pore allowing potassium ions to flow from the inside to outside of the cell down its electrochemical gradient. This flow of ions is the current, along with sodium ions flowing through analogous sodium channels, which forms nerve impulses.

One of the transmembrane segments, S4, is known as the "voltage sensor" and contains seven positively charged amino acids. These charges feel a force due to the transmembrane potential and hence are likely to move in response to changes in the potential. A second segment, S2, also contains some positively charged residues and likely plays a secondary role in voltage sensing as well. Fundamental questions remain regarding how the channel senses and responds to voltage in the membrane.

For labeling the channel, a single engineered cysteine was introduced at various positions in the S3-S4 linker, near the top of the S4. Each channel therefore contains 4 cysteines, one on each subunit. Conveniently, the *Shaker* channel does not contain native cysteines that are reactive to extracellularly applied probes. Channels were expressed in Xenopus oocytes and labeled with a mixture of donor and acceptor probes, the donor in excess to ensure that most channels contain at most only one acceptor. Under this condition, two different donor-acceptor distances are expected (Fig 12b). A donor sees an acceptor on a contiguous subunit (distance R_{SC}) or on a subunit across the pore (distance R_{SA}). To measure these distances, we focused on measuring the sensitized emission lifetime. This has the great advantage that those channels containing all donors -- the majority of channels -- do not contribute signal and can be ignored. (Those containing all acceptors can also be ignored, although this is a very small fraction of the channels.) We therefore expect the sensitized emission lifetime to be bi-exponential, with the shorter lifetime corresponding to the greater E and shorter distance. Fig. 13a shows this behavior for a probe labeled at position 346. The two distances are in excellent agreement with the expected Pythagorean relationship. By placing probes at various positions, ranging from 363 near the top of S4, to 346 near the middle of the S3-S4 linker, we found that the intersubunit distances decreased. This implies that S3-S4, (and perhaps S4), is tilted towards the pore as one moves in the extracellular direction.

In FRET, and to a certain extent in LRET, absolute distances are always more difficult to measure than relative distances. However, to check whether our absolute distances were reasonable, we measured distances between residues 425. This residue is found in the crystal structure of the KcsA channel, a (non-voltage-gated) prokaryotic analog of Shaker containing two transmembranes per subunit, analogous to S5 and S6. We found R_{SA} = 30 Å, in excellent agreement with the $C_\alpha - C_\alpha$ 29 Å distance in the crystal structure [60]. Furthermore, after publication of our LRET results, other workers measured distances using "tethered linkers" and found excellent agreement in absolute distances to our results [61]. This is in sharp contrast to the FRET results [62], which yielded much larger absolute distances. The latter probably occurred because of uncertainties in donor quantum yields, and possibly because of the κ^2 factor.

Next we measured intersubunit distances as a function of voltage. Changes in lifetime, and hence distances between site 346 near S4 are shown in Fig. 13b. Fig. 13c shows a plot of R_{SC} vs. voltage, superimposed on gating charge movement. Strikingly, the changes in distance at 346 strongly mirror gating charge movement, implying that the distances we measure at 346 are related to the charge movement in S4 – and functioning of the channel. By modeling the distance vs. voltage curve, we concluded that a large transmembrane motion did not occur [17]. Furthermore, small but statistically significant changes in distance were found at positions 350, 351, 352, where 351 moved farther apart, 350 remained unchanged, and 352 moved closer together (Fig. 14a). The simplest model to account for this non-monotonic behavior is to postulate that the S3-S4 linker is helical, and undergoes a rotation about its long axis (Fig. 14b). Since the S3-S4 linker distance changes are coupled closely to the charge movement of S4, S4

may also undergo a rotation (Fig. 14c) in response to voltage. That such small distance changes can be measured is a tribute to the power of LRET, although interpretation of such small distance changes must be made with caution. Interestingly, a rotation in ligand-gated ion channels [63, 64] and a transporter [65], has recently been measured, suggesting that helix rotation may be a general feature of membrane channels.

Recent work by MacKinnon et al. [66-68] have suggested that the potassium voltage sensing channels involves a large paddle consisting of S4 and part of S3. While this does not match with LRET results mentioned above, future experiments using LRET will likely help settle any discrepancies between the two models.

Smooth Muscle ADP Swing:

We have also used LRET to study the conformational changes that occur in smooth muscle myosin for different nucleotide/actin conditions [27]. LRET provides an excellent way to measure the absolute distances of the conformational changes of myosin as it moves through its nucleotide cycle. We can alter myosin so that only one cysteine is exposed for labeling with our lanthanide probes, and then exchange on a light chain to the myosin that is labeled with an acceptor, which in this case was TMR (or Alexa-546) [27].

Muscle contractions occur due to two proteins, actin and myosin. Nucleotide-induced conformational changes within myosin cause a relative movement of myosin with respect to actin, hence converting the chemical energy in ATP into mechanical work [69-71]. However, it is unclear how, or if, these nucleotide-induced changes depend on the presence of actin. This is critical because crystal structures have been an important tool used in determining the conformation changes within myosin during its cycle, but myosin is only crystallized in the absence of actin. If there are actin-dependent conformational changes, then the current crystal structures may represent only a small subset of the actual conformational changes that occur during the catalytic cycle of myosin.

The available myosin crystal structures, as well as spectroscopic studies, of the myosin head, indicate that the myosin powerstroke arises from a relative rotation of the light chain domain of myosin with respect to the catalytic domain when the myosin undergoes a transition from an ADP-P_i state to an ADP state. However, most myosins, including smooth and cardiac muscle myosin II, all non-muscle myosin IIs, myosin V, myosin VI, and and brush border myosin I, also display an additional rotation of the light chain domain upon release of ADP when bound to actin [72, 73]. For smooth muscle myosin, this additional rotation may be necessary before ADP can be released, thereby slowing the release of ADP. Physiologically, this may be associated with the "latch" state, i.e., smooth muscle's ability to generate high tension with minimal ATP turnover.

By measuring LRET with donor lifetimes, acceptor lifetime, and donor-acceptor intensity, we were able to explore the different myosin conformations in the presence and absence of actin [27]. Figure 15 shows TMR's (the acceptor) intensity for the nucleotide/actin conditions of myosin. The D-A (donor-acceptor) +ADP+AlF_4 (or BeF_3) state (also referred to as the trapped state) shows the most energy transfer and corresponds the pre-power stroke state of the myosin before it undergoes a power stroke. AlF_4 and BeF_3 mimic a free P_i. The D-A state shows the post-power stroke state (also referred to as the rigor state) following the hydrolysis of ATP and the release of all nucleotides. As is shown in figure 15, myosin in the presence ADP or

actin are essentially the same as the rigor state. However, upon the addition of both ADP and actin, we see an increase in energy transfer. This corresponds to a state of myosin that is actin dependent. Figure 16 also shows the acceptor lifetime (or sensitized lifetime) for the same system. Once again the trapped states show the shortest lifetime and hence the most energy transfer, while the rigor, ADP, and actin state show have the longest lifetime and correspond to the least energy transfer. Upon the addition of actin and ADP, there is a slight increase in energy transfer corresponding to the ADP state of smooth muscle myosin. Donor lifetimes show the same result, but are not shown here.

Final Remarks

New biophysical techniques invariable open up new applications. The development of new probes is leading to a dramatic expansion of the use of fluorescence in general, and FRET-(LRET)-based techniques in particular. The most pressing issue is the ability to site-specifically label probes. Temporal and spectral discrimination when using lanthanides in energy transfer measurements help decrease the sensitivity to non-specific labeling. However, particularly for cellular work, more selective means of attachments for both donors and acceptors are needed. Two different methods, one for donor, and one for acceptor, would be ideal. Genetically encoded dyes such as Green Fluorescent Proteins is one method of selective attachment [74]; dyes such as "FLASH", which bind to a highly unusual six amino acid motive via an aresenic moiety, is another [75]; dyes modified to contain Ni, which can then coordinate to a hexahistidine group engineered into a protein is yet another [76]. Using the power of these new labeling methods with the power of lanthanides will likely shed new light on biophysical systems in the near future.

Acknowledgments.

This work was supported by NIH AR44420, NSF 9984841, and through the Material Research Laboratory, Univ. of Illinois, DOE grant DEFG 02-91ER45439.

Figure 1. Structure of representative chelates: a) figure of Tb-DTPA-cs124 b) Terpyridine with Eu^{3+} bound.

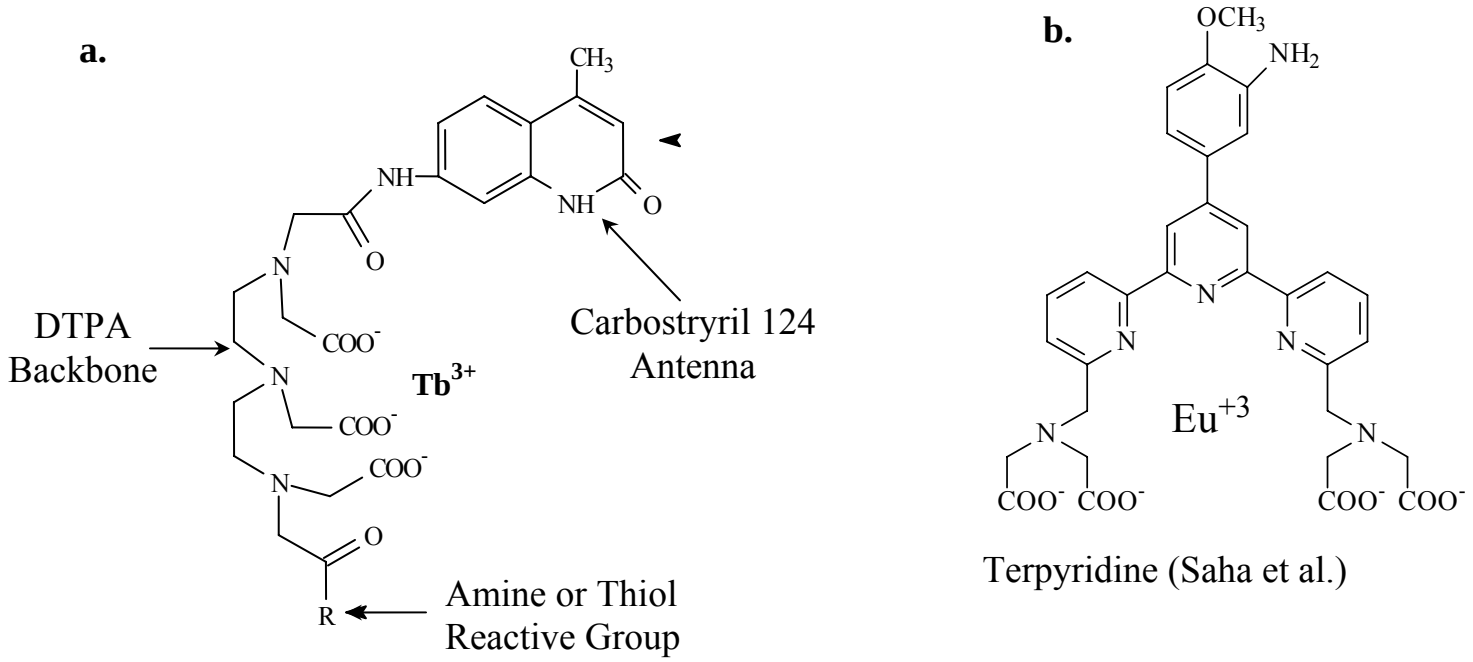

Fig. 2. a) Emission spectra and b) lifetime of Tb^{3+}- and Eu^{3+} – DTPA-cs124.

a.

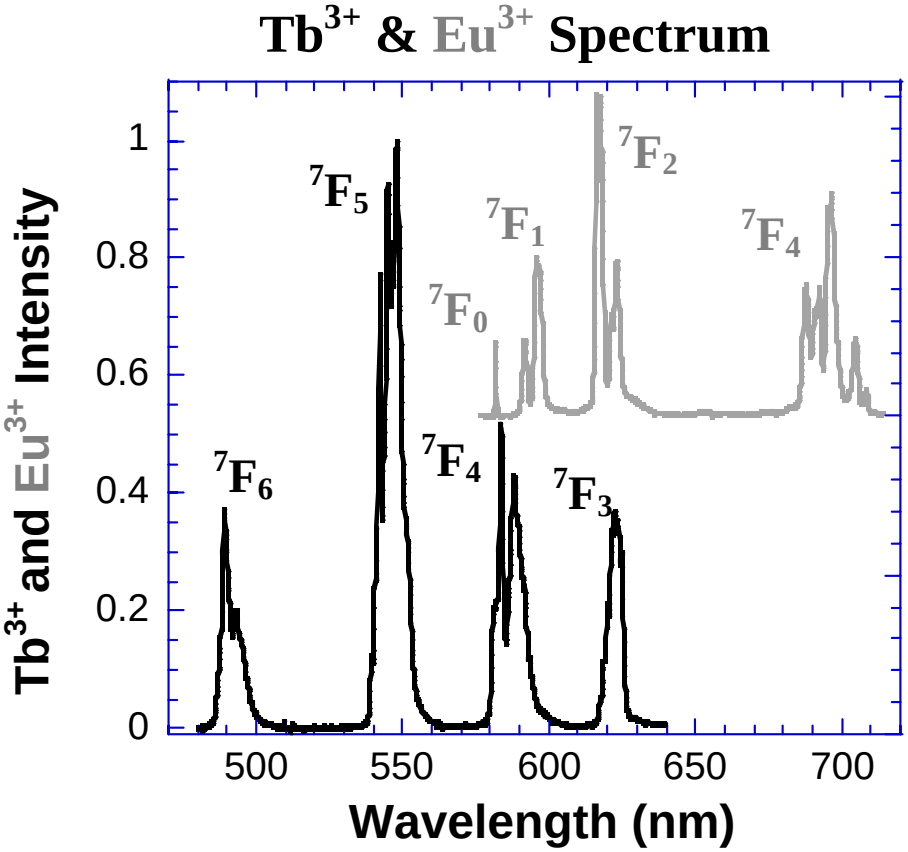

b.

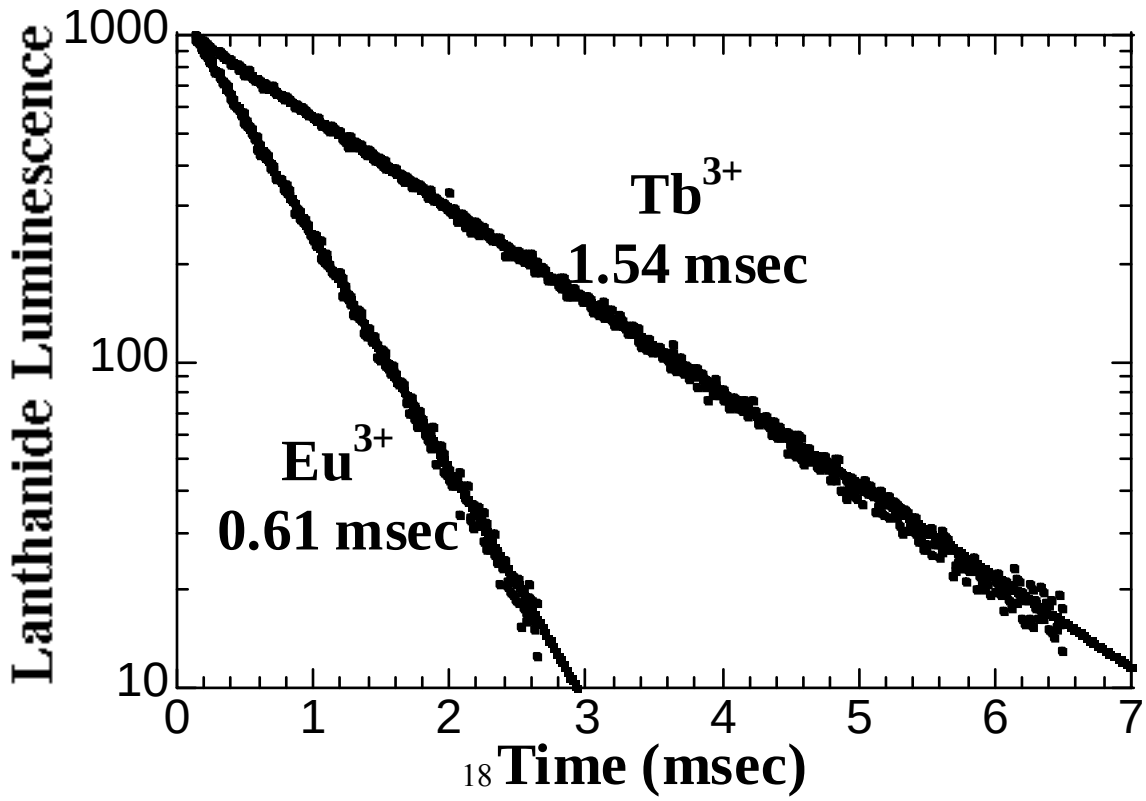

Figure 3: Anisotropy of Eu-DTPA-cs124 for the four major transitions within Eu^{3+}

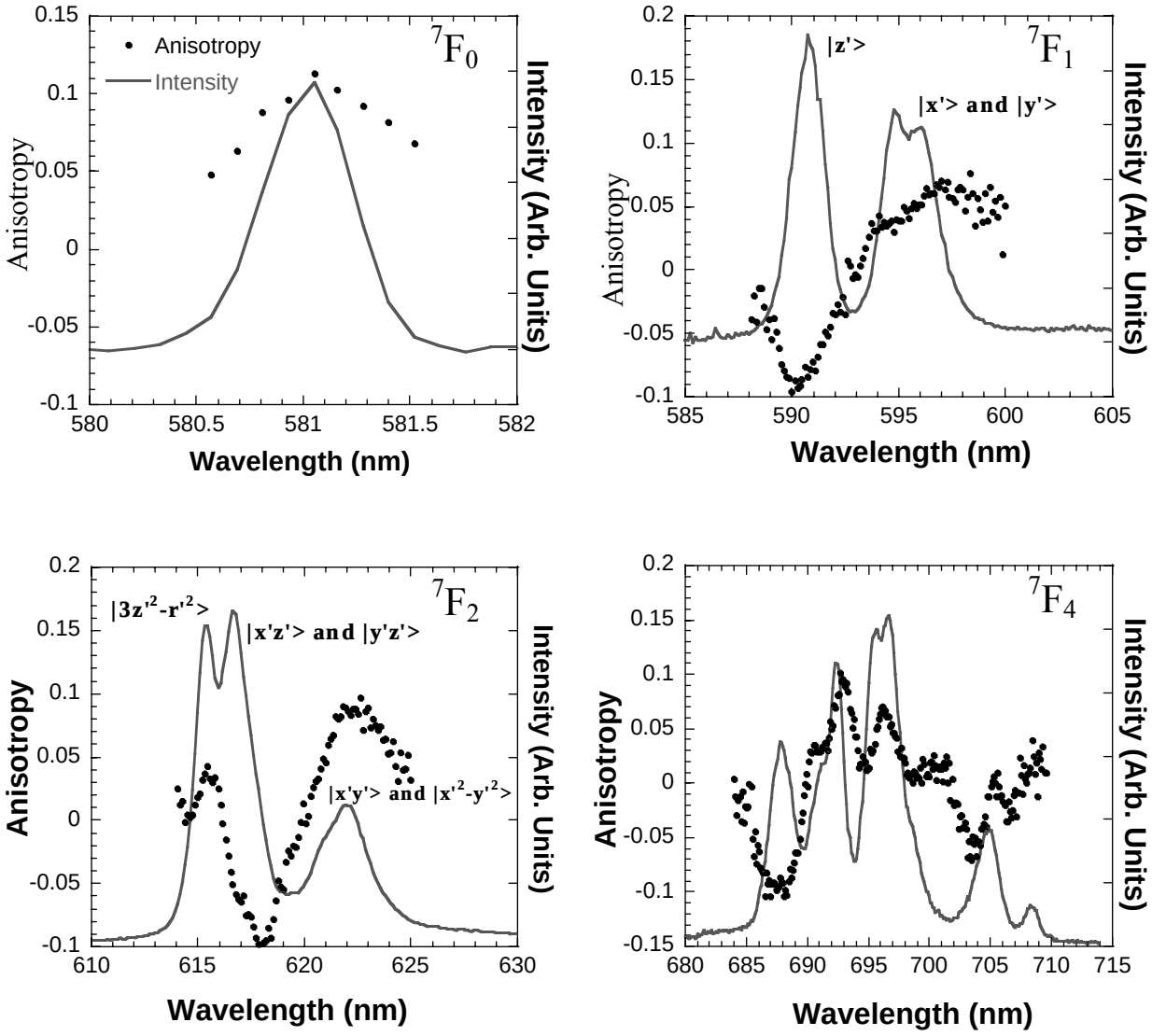

Figure 4: Anisotropy of Tb-DTPA-cs124 for the four major transitions within Tb^{3+}

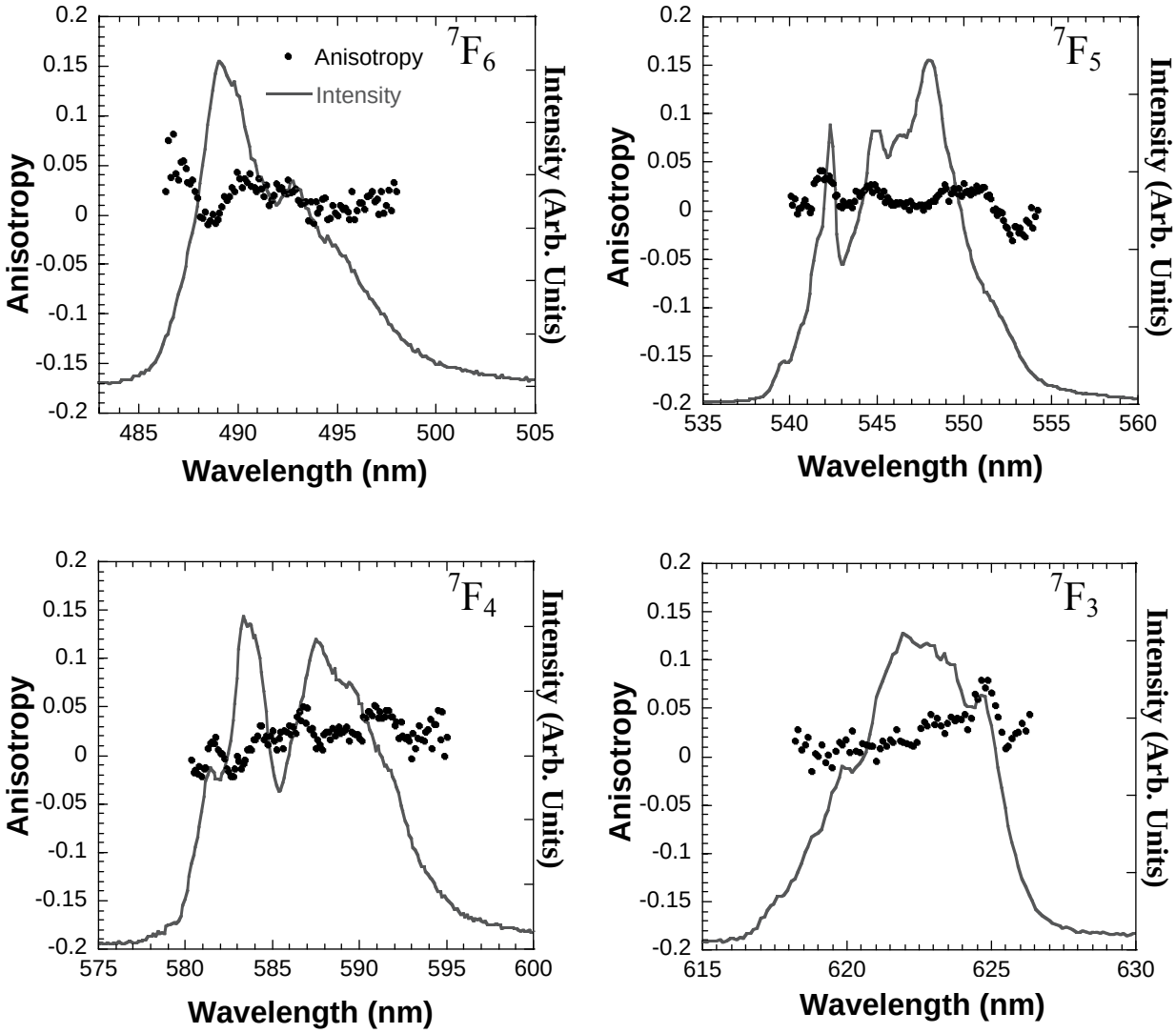

Figure 5: Definition of quantum yields.

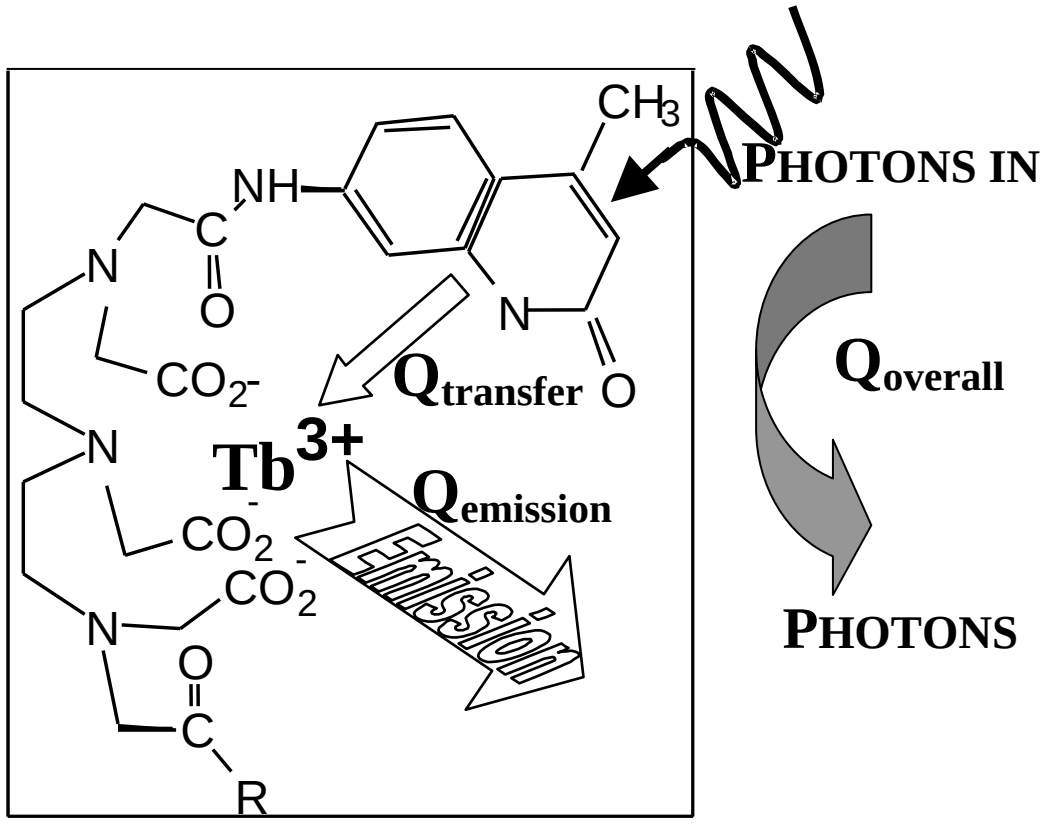

Fig 6: Amine reactive chelate complexes

a.

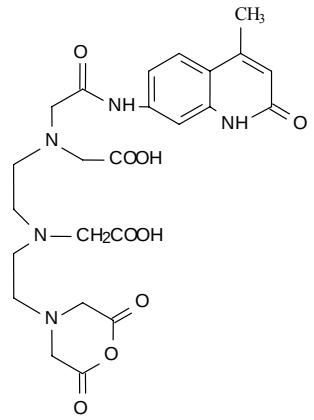

AR1

b.

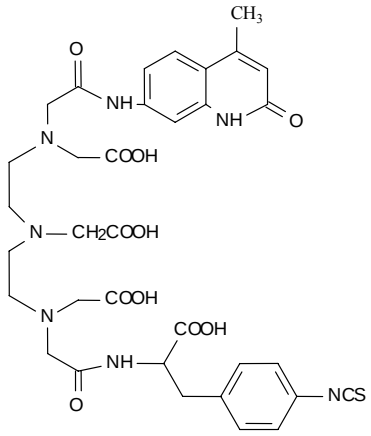

AR2

Fig 7: Thiol reactive chelate complexes

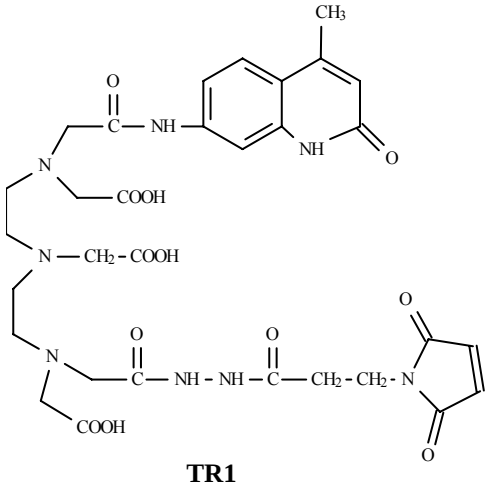

TR1

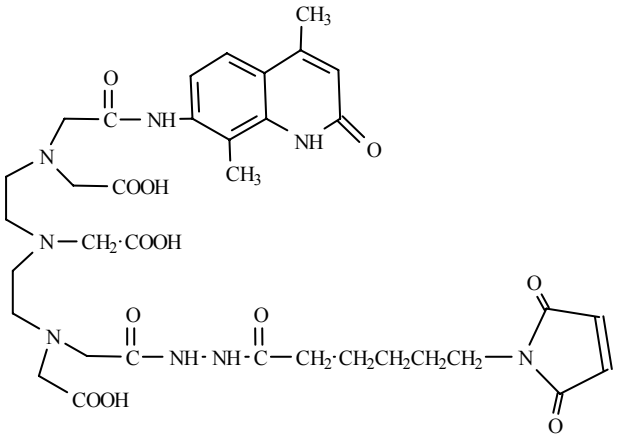

TR2

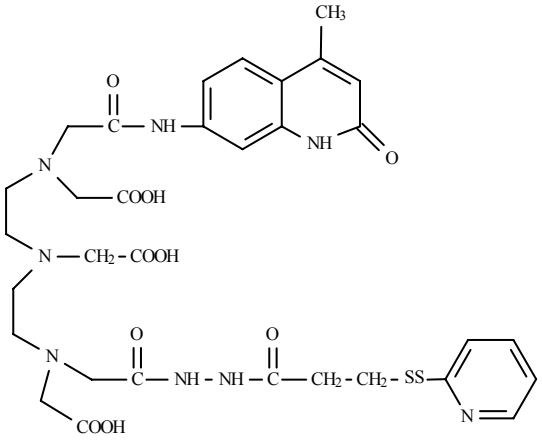

TR3

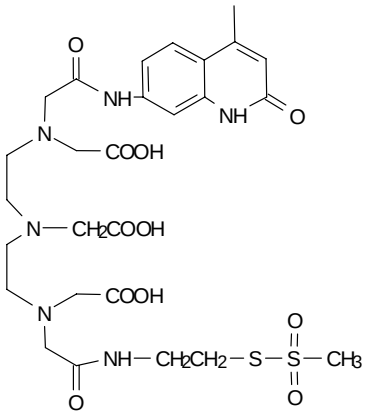

TR4

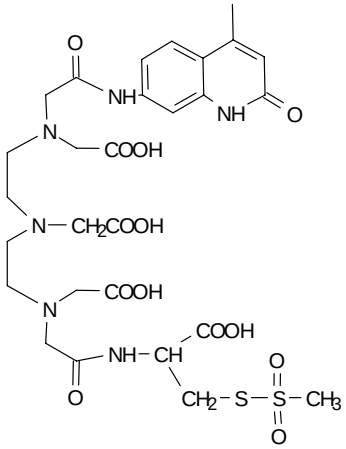

TR5

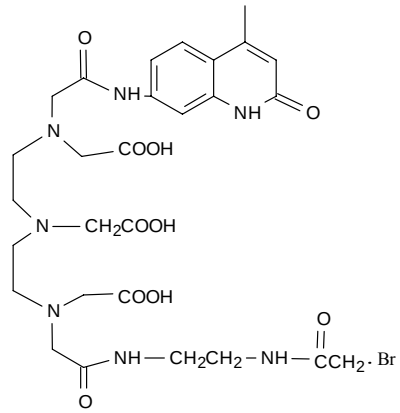

TR6

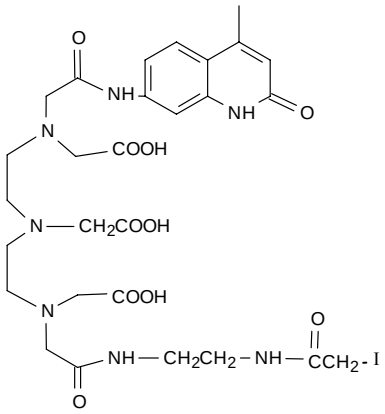

TR7

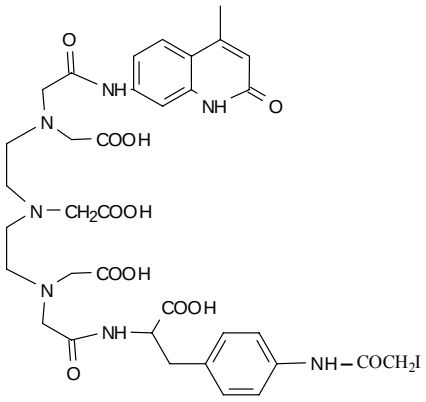

TR8

Figure 8: Different chelates used in the lanthanide antenna complexes.

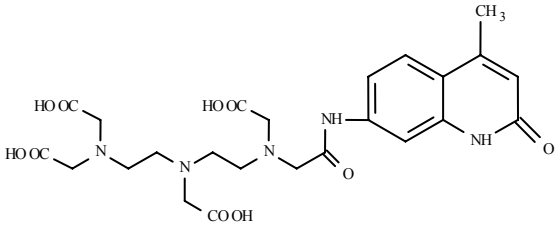

DTPA-cs124

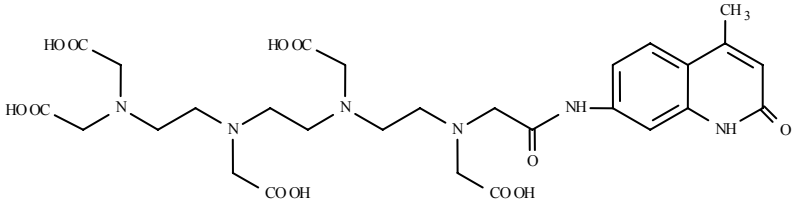

TTHA-cs124

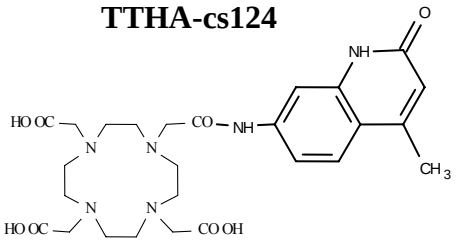

DOTA-cs124

Figure 9: Carbostyril Derivatives

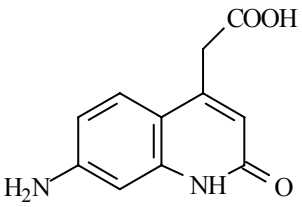

d1

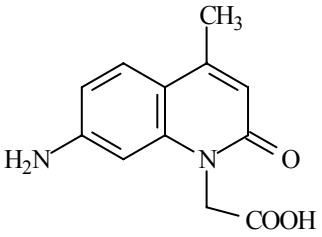

d2

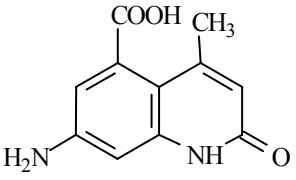

d3

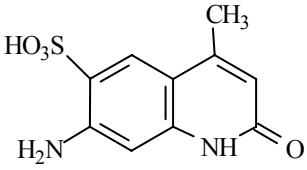

d4

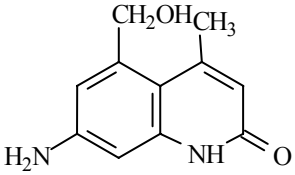

d5

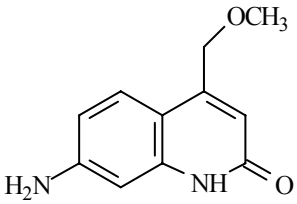

d6

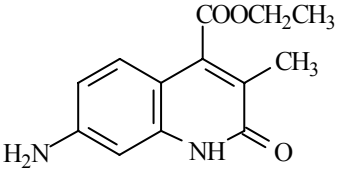

d7

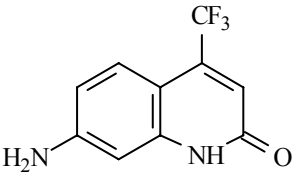

d8

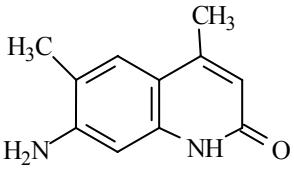

d9

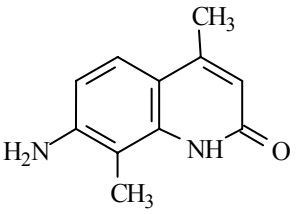

d10

Fig. 10: a) DNA Hybridization and model system for LRET. **b)** Lifetime data. **c)** Spectral data. (Figure adapted from [50]).

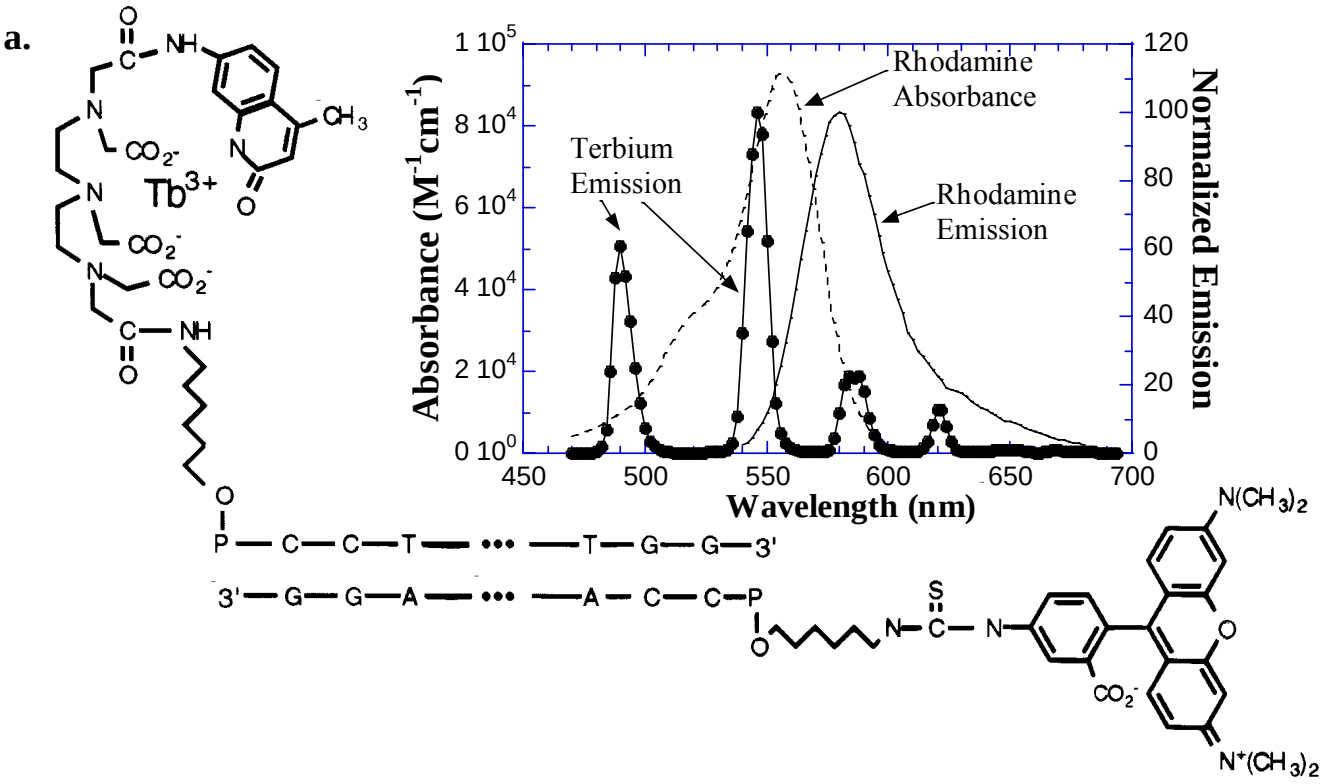

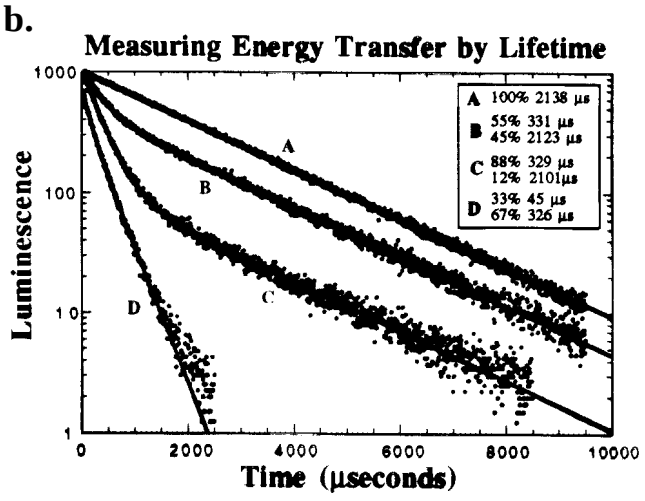

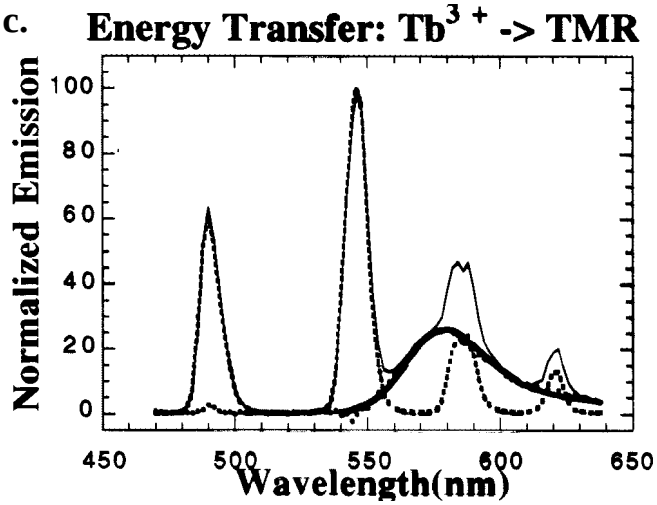

Fig. 11: LRET Instrumentation. A pulsed nitrogen laser excites the lanthanide sample, and emission is collected by a mechanically-chopped spectrometer and CCD for time-delayed spectral measurements, or a spectrometer and electronically-gated PMT for excited-state lifetime measurements. (Figure from [59].)

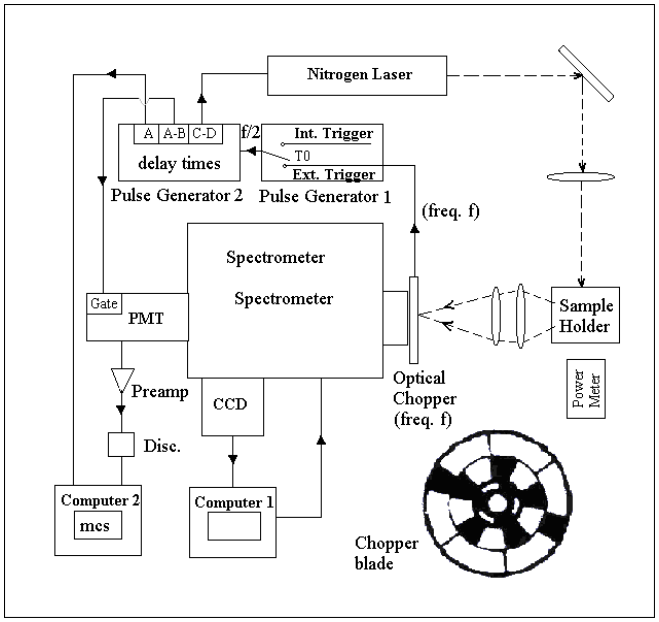

Fig. 12: Structure of Shaker potassium ion channel and labeling scheme. **a.** Side view, **b.** top view, **c.** sub-structure. The channel consists of a central pore (red in 6a) surrounded by four identical subunits. Each subunit consists of six transmembrane domains (6c) and is labeled with either a donor (blue, 6a,b), or acceptor (green, 6a,b). Labeling is done such that there are 3 donors (blue) and only one acceptor (green) per channel. Specific labeling is achieved by introducing a unique cysteine in the S3-S4 linker, near S4, which is the voltage sensor.

a.

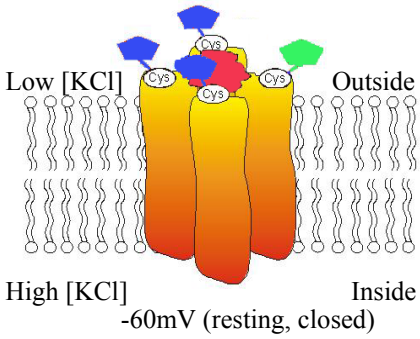

b.

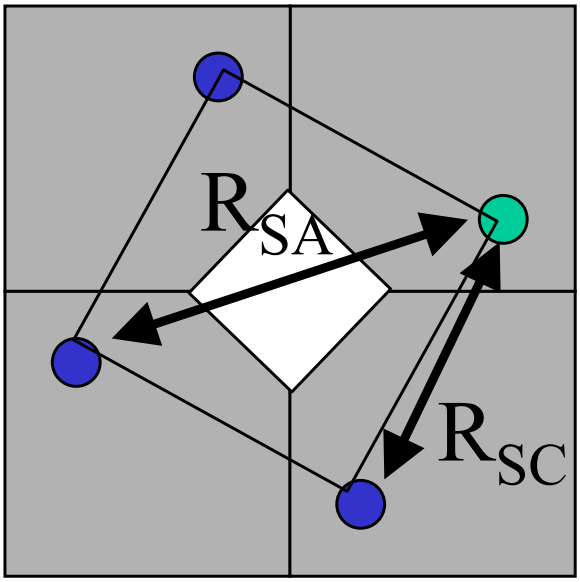

c.

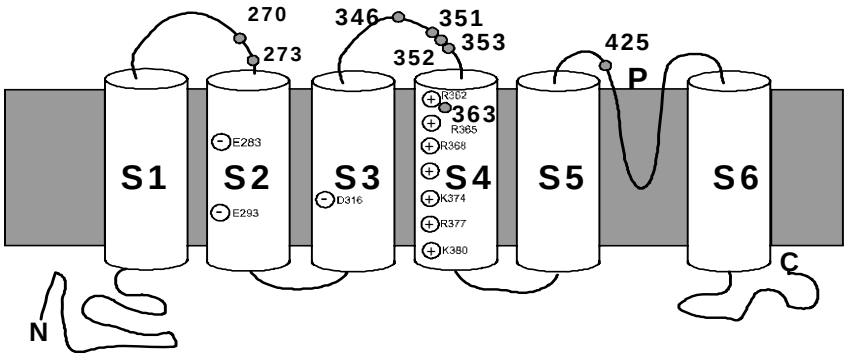

Fig. 13: a. Biexponential sensitized emission, corresponding to two donor-acceptor distances, corresponding to distances between subunits across the channel and neighboring subunits. **b.** Voltage-dependent changes in sensitized emission arising from movement of S346C in the voltage-sensing region of Shaker potassium channel. **c.** Changes in distance between S346 and amount of charge in S4 moved across membrane potential. The changes in distance closely mirror the charge movement in S4. (Figures from [17].)

a.

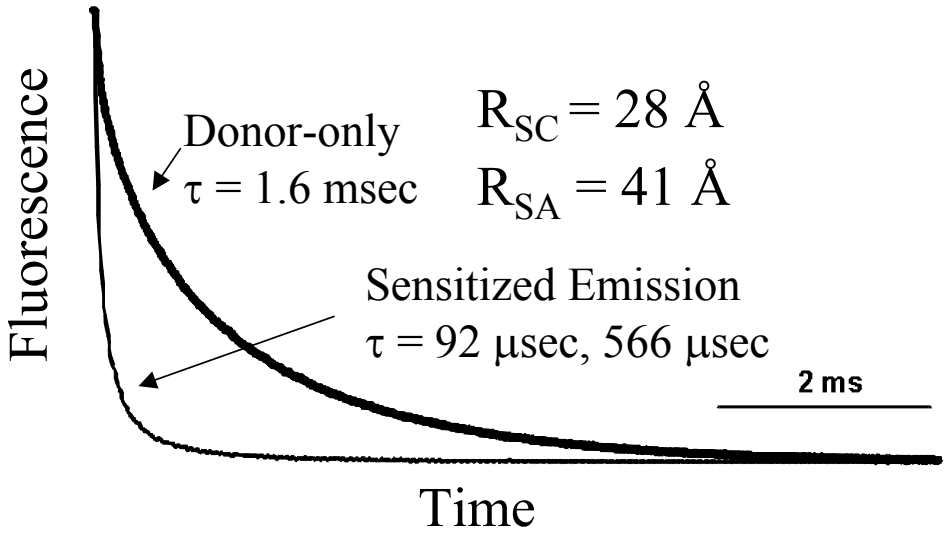

b.

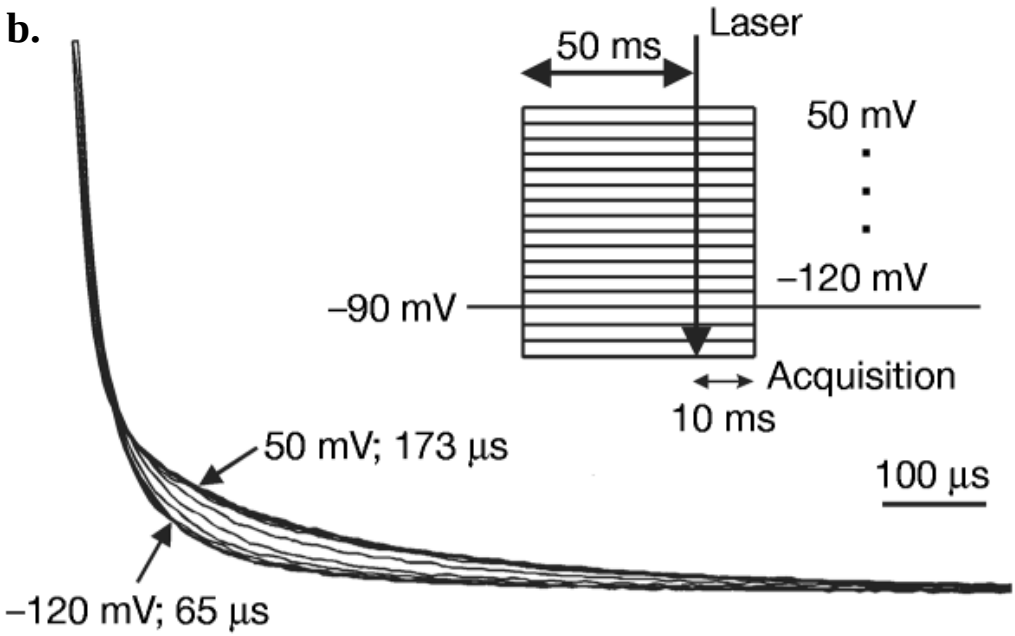
Laser
50 ms
50 mV
−120 mV
−90 mV
Acquisition
10 ms
50 mV; 173 µs
100 µs
−120 mV; 65 µs

c.

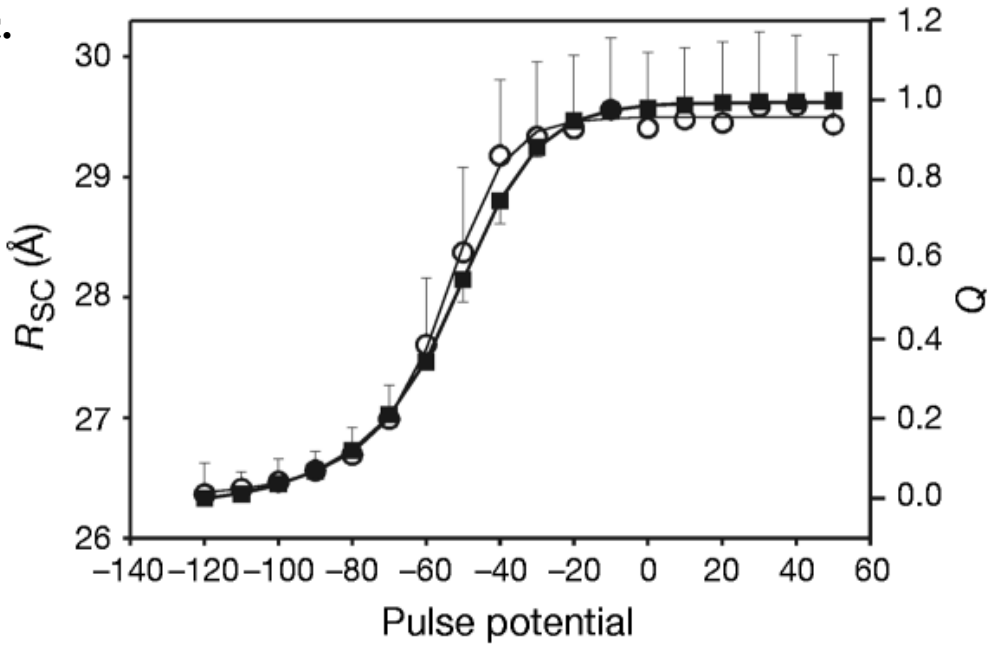
R_{SC} (Å)
Q
Pulse potential
30
29
28
27
26
1.2
1.0
0.8
0.6
0.4
0.2
0.0
−140 −120 −100 −80 −60 −40 −20 0 20 40 60

Fig. 14: Changes in distance between sites 351-353. These data can be explained by a rotation of a helical segment of the ion channel (b), leading to a model where the voltage sensor, S4, may undergo a rotation in response to voltage (c). (Adapted from [17, 62].

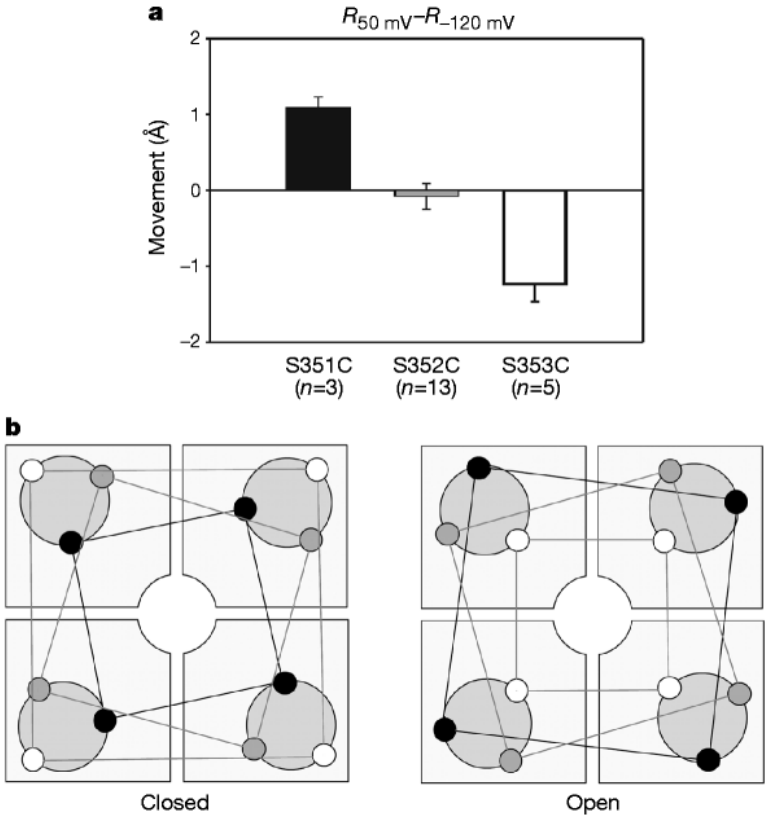

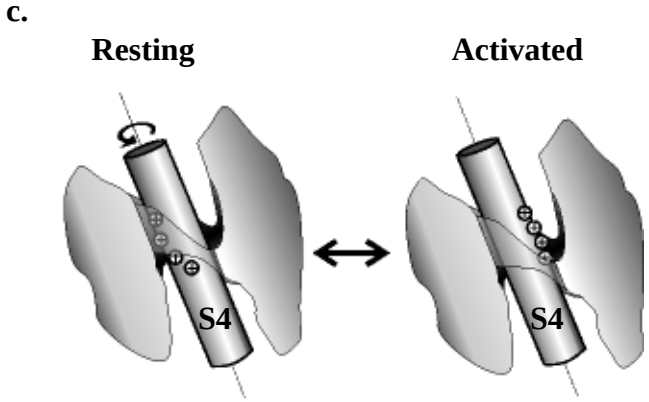

Figure 15: CCD (or spectra) measurements of LRET for smooth muscle myosin II.

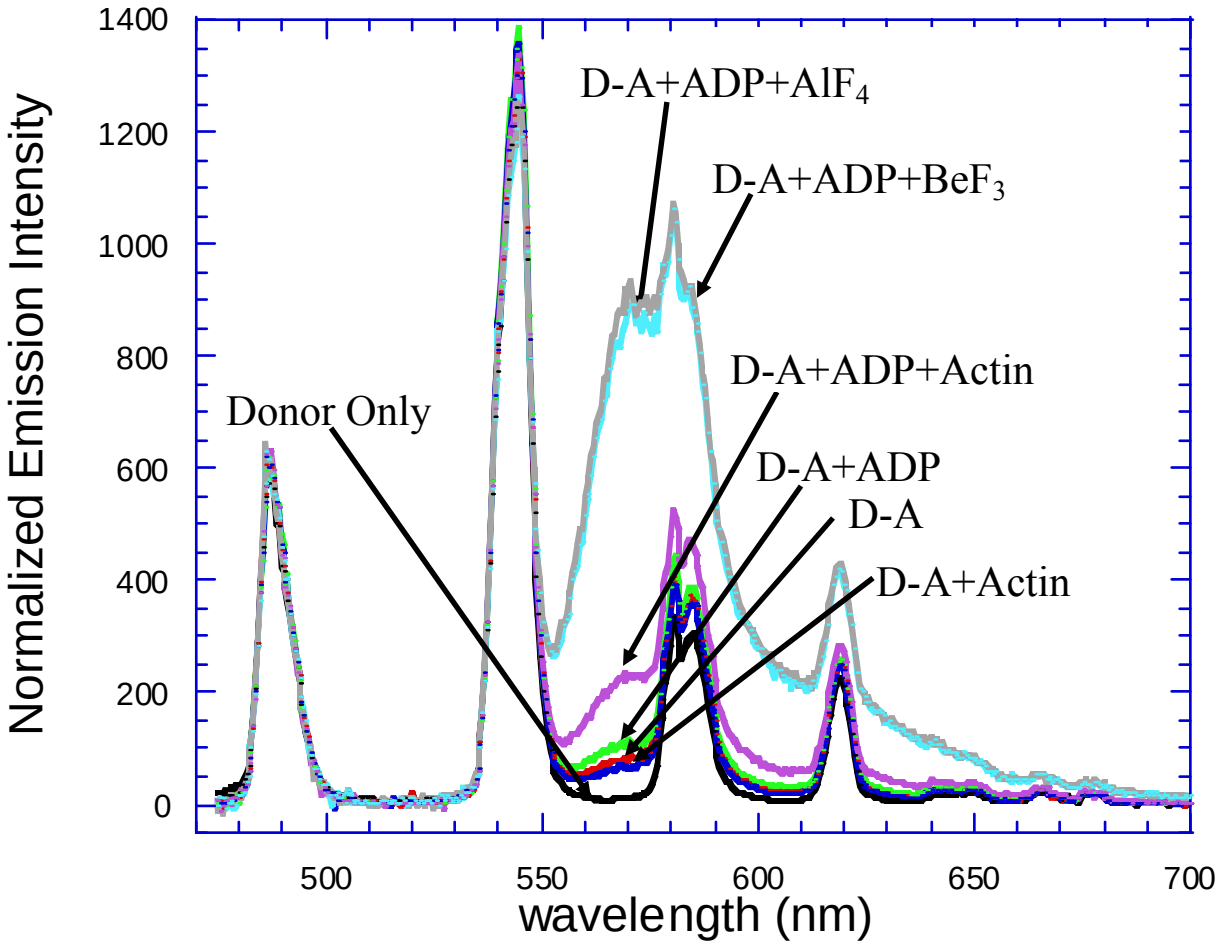

Figure 16: Sensitized lifetime for smooth muscle myosin II.

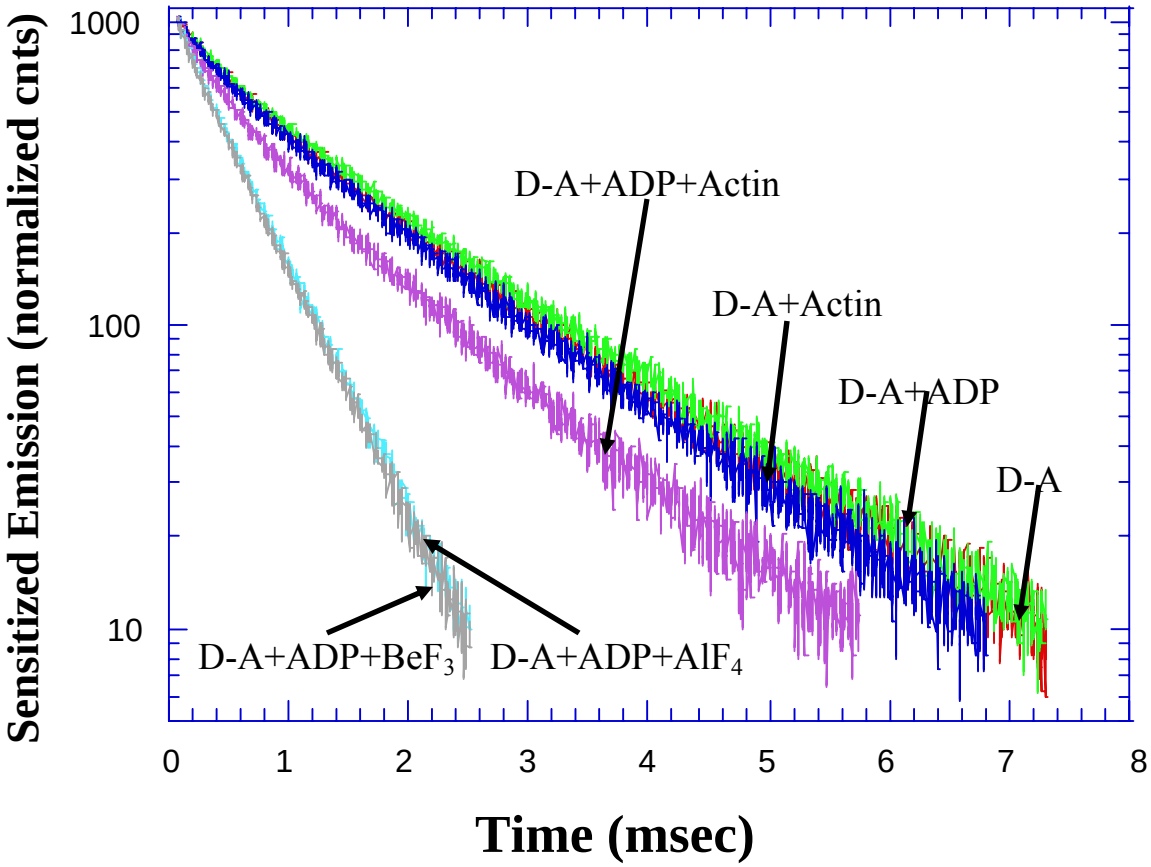

Table 1. Lifetimes and the Number of Waters Coordinated in the Inner Sphere of Lanthanide Chelates

Complexes Tb(Eu)	τ_{H_2O} (ms)	τ_{D_2O} (ms)	τ_{H_2O}/ τ_{D_2O}	**No. of waters**	Relative intensity
DTPA-cs124	1.55 (0.62)	2.63 (2.42)	0.59 (0.26)	1.1 (1.26)	1 (1)
TTHA-cs124	2.10 (1.19)	2.37 (1.79)	0.89 (0.66)	0.2 (0.3)	1.1 (2.67)
DOTA-cs124	1.54 (0.62)	2.61 (2.25)	0.59 (0.27)	1.1 (1.23)	1.1 (0.66)

Table 2. Brightness and lifetimes of Tb^{3+} and Eu^{3+} complexes of cs124 derivative chelates

Metal	Chelate	Relative Brightness (%)	Lifetimes (ms)
Tb^{3+}	DTPA-cs124 ("Benchmark")	100	1.53
	DTPA-**d4**	62	1.58
	DTPA-**d4**-EMCH	72	1.86 76%; 0.44 24%
	DTPA-**d10**	80	1.74
	DTPA-**d10**-EMCH	58	2.16 82%; 0.92 18%
	DTPA-**d10**-EDA-Br	64	1.68
	DTPA-**d5**	79	0.93 45%; 0.65 55%
	DTPA-**d5**-EMPH	37	0.82 85%; 0.37 15%
	DTPA-**d3**	36	0.82 24%; 0.50 76%
	DTPA-**d9**	87	1.63
	DTPA-**d9**-EMCH	4	1.85 59%; 0.25 41%
	DTPA-**d1**	80	1.38
	DTPA-**d6**	100	1.09
	DTPA-**d7**	N/A	N/A
	DTPA-**d2**	77	1.29
	DTPA-**d2**-EMCH	20	1.43 74%; 0.41 26%
Eu^{3+}	DTPA-cs124 ("Benchmark")	100	0.61
	DTPA-**d4**	77	0.605
	DTPA-**d4**-EMCH	22	0.42 76%; 0.14 24%
	DTPA-**d10**	100	0.603
	DTPA-**d10**-EMCH	26	0.57 60%; 0.12 40%
	DTPA-**d10**-EDA-Br	43	0.60
	DTPA-**d5**	38	0.64 68%; 0.41 32%
	DTPA-**d5**-EMPH	34	0.55 75%; 0.11 25%
	DTPA-**d3**	75	0.60
	DTPA-**d9**	60	0.605
	DTPA-**d9**-EMCH	N/A	N/A
	DTPA-**d1**	52	0.60
	DTPA-**d6**	173	0.60
	DTPA-**d7**	152	0.53
	DTPA-**d2**	100	0.60
	DTPA-**d2**-EMCH	10	0.44 68%; 0.11 32%
	DTPA-**d8**	300	0.62
	TTHA-**d8**	170	1.19

Table 3:

J-values and R_o for Lanthanide Chelates and Organic Dyes

Donor-Acceptor Pairs*	J-Value (M^{-1} cm^{-1} nm^4)	R_o (Å)
Terbium to Fluorescein (bound to DNA) (ε_{max} = 75k @ 492 nm)	9.23 x 10^{14}	45.0
Terbium to eGFP (free) (ε_{max} = 55k @ 488 nm)	7.14 x 10^{14}	43.1
Terbium to TMR (bound to DNA) (ε_{max} = 100k @ 557nm)	3.80x 10^{15}	57.0
Terbium to Cy3 (free) (ε_{max} = 150k @ 552nm)	5.82 x 10^{15}	61.2
Terbium to R phycoerythrin pH 7.5 (free) (ε_{max} = 1,960k @ 566nm)	9.60 x 10^{16}	97.5
Europium to Cy5 (bound to myosin) (ε_{max} = 249k @ 650nm)	8.89 x 10^{15}	55.2
Europium to Allophycocyanin pH 7.5 (free) (ε_{max} = 700k @ 652nm)	4.01 x 10^{16}	71.0

* J and Ro calculated for Terbium and Europium using corrected emission spectra and quantum yields for lanthanide bound to DTPA-cs124 in aqueous solutions (q_{Tb} = 0.48; q_{Eu} = 0.17). J and R_o in D_2O and in other chelates with same emission spectra can be determined by multiplying by the appropriate quantum yields, found in [24]. Other constants: n = 1.33; κ^2= 2/3. The emission spectra of Tb^{3+} and Eu^{3+} are insensitive to attachment to biomolecules although the absorption spectra of the acceptor dye can be somewhat sensitive to attachment. Absorption spectra of R phycoerythrin and Allophycocyanin are from Molecular Probes Inc., and Cy-3 from Amersham.

References

1. Seveus, L., et al., *Use of Fluorescent Europium Chelates as Labels in Microscopy Allows Glutaraldehyde Fixation and Permanent Mounting and Leads to Reduced Autofluorescence and Good Long-Term Stability.* Microscopy Res. and Technique, 1994. **28**: p. 149-154.
2. Marriott, G., et al., *Time-resolved delayed luminescence image microscopy using an europium ion chelate complex.* Biophysical Journal, 1994. **67**: p. 957-965.
3. Stryer, L., D.D. Thomas, and C.F. Meares, *Diffusion-Enhanced Fluorescence Energy Transfer*, in *Ann. Rev. of Biophys. Bioeng.*, L.J. Mullins, Editor. 1982, Annual Reviews, Inc.: Palo Alto, CA. p. 203-222.
4. Selvin, P.R., *Lanthanide-based resonance energy transfer.* IEEE J. of Selected Topics in Quantum Electronics: Lasers in Biology, 1996. **2**(4): p. 1077-1087.
5. Mathis, G., *Probing molecular interactions with homogeneous techniques based on rare earth cryptates and fluorescence energy transfer.* Clinical Chem., 1995. **41**(9): p. 1391-1397.
6. Mathis, G., *Rare earth cryptates and homogeneous fluoroimmunoassays with human sera.* Clinical Chem., 1993. **39**(9): p. 1953-1959.
7. Mathis, G., et al., *Homogeneous immunoassays using rare earth cryptates and time resolved fluorescence: principles and specific advantages for tumor markers.* Anticancer Res, 1997. **17**(4B): p. 3011-4.
8. Kolb, A.J., J.W. Burke, and G. Mathis, *A homogeneous, time-resolved fluorescence method for drug discovery*, in *High Throughput Screening: The Discovery of Bioactive Substances*, J.P. Devlin, Editor. 1997, Marcel Dekker Inc. p. 345-360.
9. Stenroos, K., et al., *Homogeneous time-resolved IL-2-IL-2R alpha assay using fluorescence resonance energy transfer.* Cytokine, 1998. **10**(7): p. 495-9.
10. Farrar, S.J., et al., *Stoichiometry of a Ligand-gated Ion Channel Determined by Fluorescence Energy Transfer.* J. Biol. Chem., 1999. **274**(15): p. 10100-10104.
11. Blomberg, K., P. Hurskainen, and I. Hemmila, *Terbium and Rhodamine as Labels in a Homogeneous Time-resolved Fluorometric Energy Transfer Assay of the B Subunit of Human Chorionic Gonadotropin in Serum.* Clinical Chemistry, 1999. **45**(6): p. 855-861.
12. Jones, S.G., et al., *Improvements in the Sensitivity of Time Resolved Fluorescence Energy Transfer Assays.* J. Fluorescence, 2001. **11**(1): p. 13-21.
13. Heyduk, E., et al., *Conformational changes of DNA induced by binding of chironomus high mobility group protein 1a (cHMG1a).* J. Biol. Chem., 1997. **272**(32): p. 19763-19770.
14. Heyduk, E. and T. Heyduk, *Architecture of a complex between the sigma70 subunit of Escherichia coli RNA polymerase and the nontemplate strand oligonucleotide. Luminescence resonance energy transfer study.* J Biol Chem, 1999. **274**(6): p. 3315-22.
15. Xiao, M., et al., *Conformational changes between the active-site and regulatory light chain of myosin as determined by luminescence resonance energy transfer: The effect of nucleotides and actin.* Proc. Nat'l. Acad. Sci., USA, 1998. **95**: p. 15309-15314.
16. Chen, J. and P.R. Selvin, *Lifetime and color-tailored fluorophores in the micro- to milli-second time regime.* J. Am. Chem. Soc., 2000. **122**(4): p. 657-660.
17. Cha, A., et al., *Atomic scale movement of the voltage sensing region in a potassium channel measured via spectroscopy.* Nature, 1999. **402**: p. 809-813.
18. Lis, S., et al., *Energy Transfer in Solution of Lanthanide Complexes.* Journal of Photochemistry & Photobiology A: Chemistry, 2002. **150**: p. 223-247.
19. Saha, A.K., et al., *Time-Resolved Fluorescence of a New Europium Chelate Complex: Demonstration of Highly Sensitive Detection of Protein and DNA Samples.* J. Am. Chem. Soc., 1993. **115**: p. 11032-11033.
20. Xu, Y.Y., et al., *Simultaneous quadruple-label fluorometric immunoassay of thyroid- stimulating hormone, 17 alpha-hydroxyprogesterone, immunoreactive trypsin, and creatine kinase MM isoenzyme in dried blood spots.* Clin Chem, 1992. **38**(10): p. 2038-43.
21. Bunzli, J.-C.G., *Luminescent Probes*, in *Lanthanide Probes in Life, Chemical and Earth Sciences, Theory and Practice*, J.-C.G. Bunzli and G.R. Choppin, Editors. 1989, Elsevier: New York. p. 219-293.
22. Drexhage, K.H., *Monomolecular Layers and Light.* Sci. Amer., 1970. **222**(3): p. 108-119.
23. Reifenberger, J., et al., *Emission Polarization Properties of Europium and Terbium Chelates.* J. Phys. Chem B, 2003. **107**: p. 12862-12873.

24. Xiao, M. and P.R. Selvin, *Quantum Yields of Luminescent Lanthanide Chelates and Far-Red Dyes Measured by Resonance Energy Transfer.* J. Am. Chem. Soc., 2001. **123**: p. 7067-7073.
25. Li, M. and P.R. Selvin, *Amine-reactive forms of a luminescent DTPA chelate of terbium and europium: Attachment to DNA and energy transfer measurements.* Bioconjugate Chem., 1997. **8**(2): p. 127-132.
26. Chen, J. and P.R. Selvin, *Thiol-reactive luminescent lanthanide chelates.* Bioconjugate Chem., 1999. **10**(2): p. 311-315.
27. Xiao, M., et al., *An actin-dependent conformational change in myosin.* Nat Struct Biol, 2003. **10**(5): p. 402-8.
28. Akabas, M.H., et al., *Acetylcholine receptor channel structure probed in cysteine-substitution mutants.* Science, 1992. **258**: p. 307-310.
29. Ge, P. and P.R. Selvin, *Thiol-reactive Lanthanide Chelates, II.* Bioconjugate Chemistry, 2003. **14**: p. 870-876.
30. Ge, P. and P.R. Selvin, *Carbostyril Derivatives as Antenna Molecules for Luminescent Lanthanide Chelates.* Bioconjugate Chemistry, 2004.
31. Schelte, P., et al., *Differential reactivity of maleimide and bromoacetyl functions with thiols: application to the preparation of liposomal diepitope constructs.* Bioconjug Chem, 2000. **11**(1): p. 118-23.
32. Li, M. and P.R. Selvin, *Luminescent lanthanide polyaminocarboxylate chelates: the effect of chelate structure.* J. Am. Chem. Soc., 1995. **117**: p. 8132-8138.
33. Chen, J. and P.R. Selvin, *Synthesis of 7-Amino-4-trifluoromethyl-2-(1H)-quinolinone and its use as an antenna molecule for luminescent europium polyaminocarboxylate chelates.* J. Photochem. Photobio. A:Chemistry, 2000. **5522**: p. 1-6.
34. Crosby, G.A., R.E. Whan, and R.M. Alire, *Intramolecular energy transfer in rare earth chelates: the role of the triplet state.* J. Chem. Phys., 1961. **34**: p. 743.
35. Abusaleh, A. and C. Meares, *Excitation and De-Excitation Processes in Lanthanide Chelates Bearing Aromatic Sidechains.* Photochemistry and Photobiology, 1984. **39**(6): p. 763-769.
36. Kirk, W.R., W.S. Wessels, and F.G. Prendergast, *Lanthanide-Dependent Perturbations of Luminescence in Indolylethylenediaminetetraacetic Acid-Lanthanide Chelate.* J. Phys. Chem., 1993. **97**: p. 10326-10340.
37. Alpha, B., et al., *Antenna Effect in Luminescent Lanthanide Cryptates: A Photophysical Study.* Photochemistry and Photobiology, 1990. **52**(2): p. 299-306.
38. Horrocks, W.D., Jr. and D.R. Sudnick, *Lanthanide Ion Probes of Structure in Biology. Laser-Induced Luminescence Decay Constants Provide a Direct Measure of the Number of Metal-Coordinated Water Molecules.* J. Am. Chem. Soc., 1979. **101**(2): p. 334-350.
39. Horrocks, W.D., Jr., B. Holmquist, and B.L. Vallee, *Energy transfer between Terbium(III) and Cobalt(II) in thermolysins: A new class of metal-metal distance probes.* Proc. Nat. Acad. Sci. USA, 1975. **72**(12): p. 4764-4768.
40. Horrocks, W.D., Jr. and D.R. Sudnick, *Lanthanide Ion Luminescence Probes of the Structure of Biological Macromolecules.* Accounts of Chemical Research, 1981. **14**: p. 384-392.
41. Selvin, P.R., *Principles and Biophysical Applications of Luminescent Lanthanide Probes. Annual Review of Biophysics and Biomolecular Structure*, 2002. **31**: p. 275-302.
42. Selvin, P.R., *The Renaissance in Fluorescence Resonance Energy Transfer.* Nature Structural Biology, 2000. **7**(9): p. 730-734.
43. Lakowicz, J.R., *Principles of Fluorescence*. 2 ed. 1999, New York: Kluwer Academic.
44. Selvin, P.R., *Fluorescence Resonance Energy Transfer*, in *Methods in Enzymology*, K. Sauer, Editor. 1995, Academic Press: Orlando. p. 300-334.
45. Förster, T., *Experimental and Theoretical Investigation of the Intermolecular Transfer of Electronic Excitation Energy.* Z. Naturforsch A, 1949. **4**: p. 321-327.
46. Chakrabarty, T., et al., *Holding two heads together: stability of the myosin II rod measured by resonance energy transfer between the heads.* Proc Natl Acad Sci U S A, 2002. **99**(9): p. 6011-6.
47. Dale, R.E., J. Eisinger, and W.E. Blumberg, *The orientational freedom of molecular probes.* Biophys. J., 1979. **26**: p. 161-194.
48. Stryer, L. and R.P. Haugland, *Energy Transfer: A Spectroscopic Ruler.* Proc. Natl. Acad. Sci., USA, 1967. **58**: p. 719-726.
49. Cantor, C.R. and P.R. Schimmel, *Biophysical Chemistry*. Vol. 2. 1980, San Francisco: W. H. Freeman and Co.

50. Selvin, P.R. and J.E. Hearst, *Luminescence energy transfer using a terbium chelate: Improvements on fluorescence energy transfer.* Proc. Natl. Acad. Sci, USA, 1994. **91**(21): p. 10024-10028.
51. Jovin, T.M. and D.J. Arndt-Jovin, *FRET microscopy: digital imaging of fluorescence resonance energy transfer. Applications in cell biology*, in *Microspectrofluorimetry of Single Living Cells*, E. Kohen, J.S. Ploem, and J.G. Hirschberg, Editors. 1989, Academic Press: Orlando. p. 99-117.
52. Heyduk, T. and E. Heyduk, *Luminescence energy transfer with lanthanide chelates: interpretation of sensitized acceptor decay amplitudes.* Anal Biochem, 2001. **289**(1): p. 60-7.
53. Weber, G. and F.W.J. Teale, *Determination of the Absolute Quantum Yield of Fluorescent Solutions.* Trans. Faraday Soc., 1957. **53**: p. 646-655.
54. Vamosi, G., C. Gohlke, and R. Clegg, *Fluorescence characteristics of 5-carboxytetramethylrhodamine linked covalently to the 5' end of oligonucleotides: multiple conformers of single-stranded and double-stranded dye-DNA complexes.* Biophys J, 1996. **71**(2): p. 972-994.
55. Karstens, T. and K. Kobs, *Rhodamine B and rhodamine 101 as reference substances for fluorescence quantum yield measurements.* J. Phys. Chem., 1980. **84**: p. 1871-1872.
56. Clegg, R.M., et al., *Observing the Helical Geometry of Double-Stranded DNA in Solution by Fluorescence Resonance Energy Transfer.* Proc. Natl. Acad. Sci. USA, 1993. **90**(7): p. 2994-2998.
57. Schobel, U., et al., *New Donor-Acceptor Pair for Fluorescent Immunoassays by Energy Transfer.* Bioconjugate Chem., 1999. **10**(6): p. 1107-1114.
58. Selvin, P.R., et al., *Crystal structure and spectroscopic characterization of a luminescent europium chelate.* Inorganic Chemistry, 1996. **35**: p. 700-705.
59. Xiao, M. and P.R. Selvin, *An Improved instrument for measuring time-resolved lanthanide emission and resonance energy transfer.* Rev. Sci. Inst., 1999. **70**(10): p. 3877-3881.
60. Doyle, D.A., et al., *The Structure of the Potassium Channel: Molecular Basis of K+ Conduction and Selectivity.* Science, 1998. **280**: p. 69-77.
61. Blaustein, R.O., et al., *Tethered blockers as molecular 'tape measures' for a voltage-gated K+ channel.* Nat Struct Biol, 2000. **7**(4): p. 309-11.
62. Glauner, K.S., et al., *Spectroscopic mapping of voltage sensor movement in the Shaker potassium channel.* Nature, 1999. **402**(6763): p. 813-817.
63. Horenstein, J., et al., *Protein mobility and GABA-induced conformational changes in GABA(A) receptor pore-lining M2 segment.* Nat Neurosci, 2001. **4**(5): p. 477-85.
64. Johnson, J.P., Jr. and W.N. Zagotta, *Rotational movement during cyclic nucleotide-gated channel opening.* Nature, 2001. **412**(6850): p. 917-21.
65. Loo, T.W. and D.M. Clarke, *Cross-linking of human multidrug resistance p-glycoprotein by the substrate, tris-(2-maleimidoethyl)amine, is altered by atp hydrolysis. Evidence for rotation of a transmembrane helix.* J Biol Chem, 2001. **276**(34): p. 31800-5.
66. Lee, S.Y. and R. MacKinnon, *A membrane-access mechanism of ion channel inhibition by voltage sensor toxins from spider venom.* Nature, 2004. **430**(6996): p. 232-5.
67. Jiang, Y., et al., *The principle of gating charge movement in a voltage-dependent K+ channel.* Nature, 2003. **423**(6935): p. 42-8.
68. Jiang, Y., et al., *X-ray structure of a voltage-dependent K+ channel.* Nature, 2003. **423**(6935): p. 33-41.
69. Rayment, I., et al., *Structure of the actin-myosin complex and its implications for muscle contraction.* Science, 1993. **261**: p. 58-65.
70. Dominguez, R., et al., *Crystal Structure of a Vertebrate Smooth Muscle Myosin Motor Domain and Its Complex with the Essential Light Chain: Visualization of the Pre-Power Stroke State.* Cell, 1998. **94**: p. 559-571.
71. Houdusse, A., et al., *Atomic Structure of Scallop Myosin Subfragment S1 Complexed with MgADP: A Novel Conformation of the Myosin Head.* Cell, 1999. **97**: p. 459-470.
72. Whittaker, M., et al., *A 35-Angstrom Movement of Smooth Muscle Myosin on ADP Release.* Nature, 1995. **378**(6558): p. 748-751.
73. Gollub, J., C.R. Cremo, and R. Cooke, *ADP release produces a rotation of the neck region of smooth myosin but not skeletal myosin.* Nature Structural Biology, 1996. **3**(9): p. 796-802.
74. Tsien, R.Y., *The green fluorescent protein.* Annu. Rev. Biochem., 1998. **67**: p. 509-44.
75. Griffin, B.A., S.R. Adams, and R.Y. Tsien, *Specific Covalent Labeling of Recombinant Protein Molecules Inside Live Cells.* Science, 1998. **281**: p. 269-272.

76. Kapanidis, A.N., Y.W. Ebright, and R.H. Ebright, *Site-specific incorporation of fluorescent probes into protein: hexahistidine-tag-mediated fluorescent labeling with (Ni(2+):nitrilotriacetic Acid (n)-fluorochrome conjugates.* J Am Chem Soc, 2001. **123**(48): p. 12123-5.